The Abdus Salam
International Centre for Theoretical Physics

United Nations
Educational, Scientific
and Cultural Organization

International Atomic
Energy Agency

SMR.1676 - 43

8th Workshop on Non-Linear Dynamics and Earthquake Prediction

3 - 15 October, 2005

Seismic Energy Release and the Prediction of Moderate Size Earthquakes at Mt. Vesuvius

Antonella Peresan
Universita di Trieste
Dipartimento di Scienze della Terra
Via E. Weiss 4
34127 Trieste
Italy

Strada Costiera 11, 34014 Trieste, Italy - Tel. +39 040 2240 111; Fax +39 040 224 163 - sci_info@ictp.it, www.ictp.it

Pure appl. geophys. 161 (2004) 123–144
0033 – 4553/04/010123 – 22
DOI 10.1007/s00024-003-2430-0

Pure and Applied Geophysics

Three Decades of Seismic Activity at Mt. Vesuvius: 1972–2000

Giuseppe De Natale,[1] Igor Kuznetzov,[2,4] Tatiana Kronrod,[2,4]
Antonella Peresan,[3] Angela Saraò,[3] Claudia Troise,[1]
and Giuliano F. Panza[3,4]

Abstract—We analyse the seismic catalogue of the local earthquakes which occurred at Somma-Vesuvius volcano in the past three decades (1972–2000). The seismicity in this period can be described as composed of a background level, characterised by a low and rather uniform rate of energy release and by sporadic periods of increased seismic activity. Such relatively intense seismicity periods are characterised by energy rates and magnitudes progressively increasing in the critical periods. The analysis of the *b* value in the whole period evidences a well-defined pattern, with values of *b* progressively decreasing, from about 1.8 at the beginning of the considered period, to about 1.0 at present. This steady variation indicates an increasing dynamics in the volcanic system. Within this general trend it is possible to identify a substructure in the time sequence of the seismic events, formed by the alternating episodes of quiescence and activity. The analysis of the source moment tensor of the largest earthquakes shows that the processes at the seismic source are generally not consistent with simple double-couples, but that they are compatible with isotropic components, mostly indicating volumetric expansion. These components are shown to be statistically significant for most of the analysed events. Such focal mechanisms can be interpreted as the effect of explosion phenomena, possibly related to volatile exsolution from the crystallising magma.

The availability of a reduced amount of high quality data necessary for the inversion of the source moment tensor, the still limited period of systematic observation of Vesuvius micro-earthquakes and, above all, the absence of eruptive events during such interval of time, cannot obviously permit the outlining of any formal premonitory signal. Nevertheless, the analysis reported in this paper indicates a progressively evolving dynamics, characterised by a generally increasing trend in the seismic activity in the volcanic system and by a significant volumetric component of recent major events, thus posing serious concern for a future evolution towards eruptive activity.

Key words: Seismicity, microearthquakes, earthquake-source mechanism, earthquake catalogue, *b* values, Vesuvius.

[1] Osservatorio Vesuviano, Napoli, Italy.
[2] Russian Academy of Sciences. International Institute of Earthquake Prediction Theory and Mathematical Geophysics, Moscow, Russian Federation.
[3] Department of Earth Sciences, University of Trieste, Trieste, Italy.
E-mail: anto@dst.units.it
[4] The Abdus Salam International Centre for Theoretical Physics – ICTP, Miramare, Trieste, Italy.

Introduction

Somma-Vesuvius is probably the most famous volcano in the world, mainly due to its large plinian eruption in Roman times (79 A.D.), which completely buried the towns of Herculaneum and Pompeii under several meters of pyroclastic and mud flows. Today, the risk of eruptions at Somma-Vesuvius is the highest in the world, because more than 700,000 people live within a radius of 10 km from the crater, an area with the maximum hazard for pyroclastic flows from plinian and subplinian eruptions. The eruptive activity of this volcano appears composed of main cycles, which start with plinian or subplinian eruptions and, after centuries of mainly effusive to moderate explosive activity, terminate with an eruption which closes the conduit (no magma in the crater anymore) (SANTACROCE, 1987). The last eruptive cycle started in 1631, with a violent subplinian eruption (ROLANDI *et al.*, 1993; ROSI *et al.*, 1993; SCANDONE *et al.*, 1993), and ended in 1944, when the last, modest, eruption closed the main conduits. According to several observations and volcanological models (SANTACROCE, 1987) the next eruption, which should open a new eruptive cycle, has a considerable probability of being a subplinian or plinian one. The very strong concern for a future eruption of this kind compelled the Italian government to prepare an evacuation plan of the whole area, in case the scientific monitoring network should record signals of an impending eruption. The careful analysis of geophysical data at this area is then of extreme importance, both for the high scientific interest of the area, and for the extreme risk involved. The main obstacle for the forecast of a future eruption in this area is the preponderant lack of knowledge regarding the precise dynamics before violently explosive eruptions. We historically reference the Roman and Spanish chronicles of the 79 and 1631 eruptions (ROSI *et al.*, 1993), but they are obviously not very useful for comparisons with the outputs from modern monitoring techniques. Several historical studies point out the lack of very high magnitude earthquakes before the eruptions (SIGURDSSON *et al.*, 1985; ROSI *et al.*, 1993), with the possible exception of an event which occurred in 62 A.D. 17 years before the 79 eruption (MARTURANO and RINALDIS, 1995). It is, however, not yet clear if such an event was really a Vesuvius event, or rather one which occurred in the neighbouring tectonic areas of the Apennine chain.

For all these reasons it is very important to study the seismic catalogue, including also relatively low magnitude events, since the expected magnitudes before eruptions will probably not exceed $M_d = 4$, i.e., they will be of the same size as those recorded in recent years. Despite the importance of the study and interpretation of seismicity in this area, it is only in recent years that various papers have been devoted to the modelling of the seismicity of the Vesuvian area (VILARDO, 1996; CAPUANO *et al.*, 1999; IANNACCONE *et al.*, 2001; MARZOCCHI *et al.*, 2001; VILARDO *et al.*, 2002). Recently, DE NATALE *et al.* (2000) presented a model to explain the mechanisms of the background seismic activity at central volcanoes, with particular reference to Somma-Vesuvius. BERRINO *et al.* (1993) reported the last integrated analysis of geophysical data collected in this area in

20 years of seismic and geodetic monitoring. Recent research on Somma-Vesuvius has been particularly devoted to the determination of the internal structure, in the framework of the large TOMOVES project (ZOLLO *et al.*, 1996; DE NATALE *et al.*, 1998). A close spatial relationship between the internal structure and seismic activity has been evidenced and interpreted by DE NATALE *et al.* (2000).

In this paper, we compute the focal mechanisms of the largest events ($M_d > 3.0$), using a method based on the computation of the full moment tensor of the events (SILENY *et al.*, 1992; SILENY, 1998) and we analyse the seismic catalogue of the last three decades of seismic activity at Somma-Vesuvius. The catalogue is based on the recordings at the station OVO, located at the Osservatorio Vesuviano building on Vesuvius, which was installed in 1972 and is equipped, since that time, with a three component Geotech S-13 sensor. We perform the analysis of energy release, as well as of the b value as a function of time, and we evidence a substructure in the seismicity, consisting of alternating periods of quiescence and activity that point out an increasing trend of the local seismic activity.

The Seismic Catalogue

The seismic catalogue of Vesuvius microearthquakes, hereinafter referred to as OV2, consists of a revised list of about 9000 local earthquakes recorded since 1972 at the station OVO (Fig. 1). The station, located at the site of the ancient building of Osservatorio Vesuviano, is equipped with 3 Geotech S-13 geophones, oriented along the three principal directions (N, E, V). The OVO station represents the first modern seismometer installed on the Vesuvius volcanic edifice, and the instrumentation has been unchanged since then, therefore it provides the longest homogeneous catalogue of the events which occurred at Vesuvius.

The magnitude of the events is determined from the time duration, according to DEL PEZZO *et al.* (1983), who compared recordings of aftershocks of the 1980 $M_L = 6.9$ Irpinia earthquake at the station OVO with the local magnitudes computed for the same events at the station located at Monte Mario, near Rome (National Institute of Geophysics), equipped at that time with a Wood-Anderson instrument. The magnitudes estimated for the events recorded at the OVO station range from slightly less than 0 to 3.6.

The stations equipment remained unchanged since its installation and the same magnitude type, M_d, is reported for all the events, therefore the precision of magnitudes determination is expected to be uniform in time. This allows us to consider the entire period of observations to perform the analysis of "magnitude grouping", which enables to evidentiate as to whether there are dominating values of magnitudes, due for example to a different accuracy of the amplitude measurements for events in different magnitude ranges. Such preliminary analysis is useful to choose the appropriate intervals of magnitude grouping to be considered for the frequency-

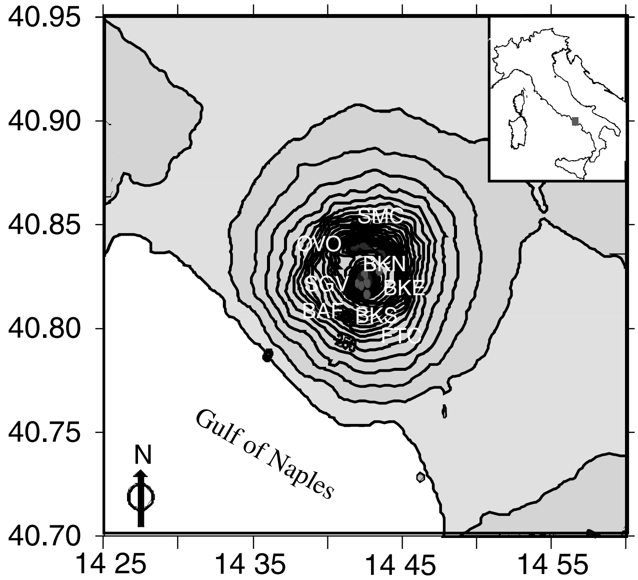

Figure 1
Somma-Vesuvius area, with contour lines and the location of the recording stations whose data have been employed in this study.

magnitude distribution; hence it is necessary both for the analysis of the catalogue completeness and for the estimation of the parameters of the frequency-magnitude relation (FMR). The distribution of the percentage of events versus magnitude is considered, with a very small magnitude step ($\Delta M = 0.1$), for three subsequent magnitude intervals: [0.4; 1.3], [1.4; 2.3] and [2.4; 3.3], as shown in Figures 2a, 2b and 2c respectively. It is possible to observe from Figure 2 that the weaker are the events, the more clear appears the magnitude grouping, i.e., some values of the decimal digit of M are more frequent than others and there are some gaps in the distribution. Thus, in the magnitude range $0.6 \le M \le 1.4$ the values 0.6, 0.9 and 1.2 appear dominant (Figs. 2a and 2b), i.e., the magnitude is grouped with the step $\Delta M = 0.3$. Similarly, for $1.5 \le \mathrm{M} \le 2.1$ the grouping step is $\Delta M = 0.2$ (values 1.5, 1.7, 1.9 are predominant, while there are gaps for 1.6, 1.8 and 2.0). The largest events, with $M \ge 2.2$, are not really grouped, i.e., they are grouped uniformly with the step $\Delta M = 0.1$ which is conditioned by the assumed format of the magnitude presentation. This analysis, repeated considering different time windows (figures are not reported), confirms that the evidenced magnitude grouping does not change in time.

The completeness of the catalogue can then be visually determined from the frequency-magnitude distribution, that is considering the distribution $\lambda(M)$ of the number of earthquakes within each magnitude grouping interval ΔM. Figure 3 shows the differential and cumulative graphs of $\log \lambda(M)$ for each of the three decades of seismic activity, normalised to the space-time-magnitude volume unit

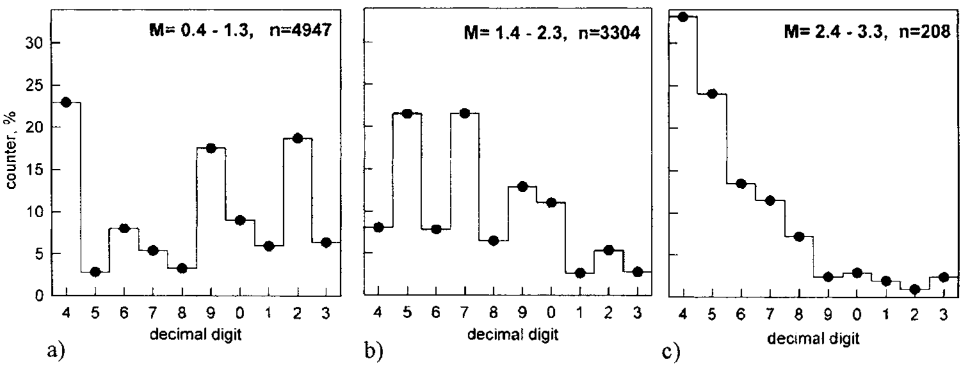

Figure 2
Distribution of the number (percentage) of events versus magnitude (decimal digit) for three adjacent magnitude intervals, considering all the events reported in the OV2 catalogue.

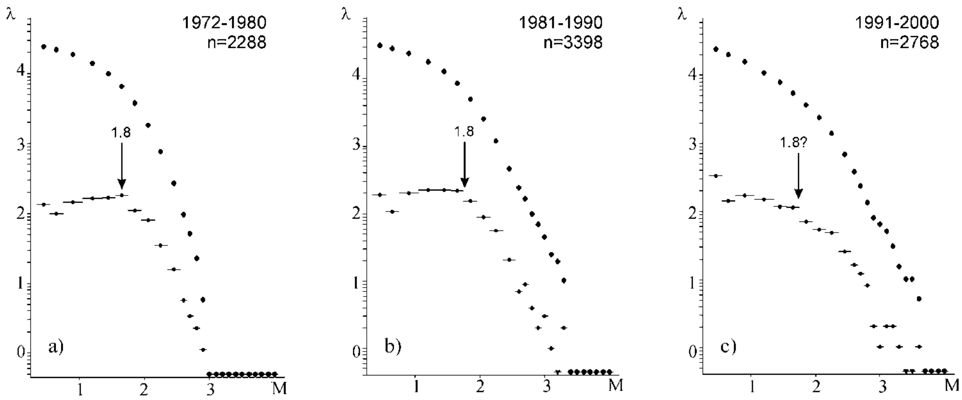

Figure 3
Differential (dots with horizontal bars) and cumulative graphs (dots) of log $\lambda(M)$ for three subsequent time periods, where λ is the number of earthquakes per space-time-magnitude volume unit $V = [1000\ km^2 \times 1\ year \times 1\ M]$. The amplitude of the magnitude grouping intervals ΔM is given by the horizontal segments, while the solid circles at their centres indicate the value of λ. The arrows indicate the selected magnitude cut-off.

$V = [1000\ km^2 \times 1\ M \times 1\ year]$. The cut-off M_{min} is fixed corresponding to the magnitude below which the empirical graph log λ(M) deviates from linearity. This set of graphs shows that the deviation from linearity appears more clearly from the non-cumulative distribution than from the cumulative one. The differential graphs log $\lambda(M)$ shown in Figures 3a and 3b indicate that the completeness magnitude cut-off can be confidently fixed at $M_{min} = 1.8$. The distribution shown in Figure 3c appears rather different: a smooth, continuous deviation from linearity is obtained instead of the abrupt change, even in the differential distribution. This difference might be related to the incomplete observations of the weaker events on the background of the stronger events (it is in this period that the strongest earthquake, with $M = 3.6$, occurred), but it might also result from a change in the seismic regime. Though the magnitude threshold for the completeness of the catalogue appears to be even lower during some limited intervals of time, we have established to keep $M_{\min} = 1.8$ for the entire period of observation and not to use a variable $M_{\min}(T)$, since we know very little about the stability of FMR at such small magnitudes. The completeness threshold $M_d = 1.8$ appears rather high for such small volcanic earthquakes; this high threshold is mainly caused by the high noise due to the urbanisation of the area.

Analysis of Seismicity

A reliable analysis of the time features of seismicity requires to consider of only the complete part of the catalogue, thus eliminating the smallest events, which are not systematically recorded. The time sequence and the yearly distribution (considering non-overlapping time windows) of the events with $M \geq 1.8$, recorded at the OVO station in the period 1972–2000, is then considered as shown in Figure 4. It is clear, from this figure, that a background seismicity is always present at Somma-Vesuvius, with a minimum rate of some tens of earthquakes per month, while periods of increased seismic activity, both in number and in magnitude of the events, can be

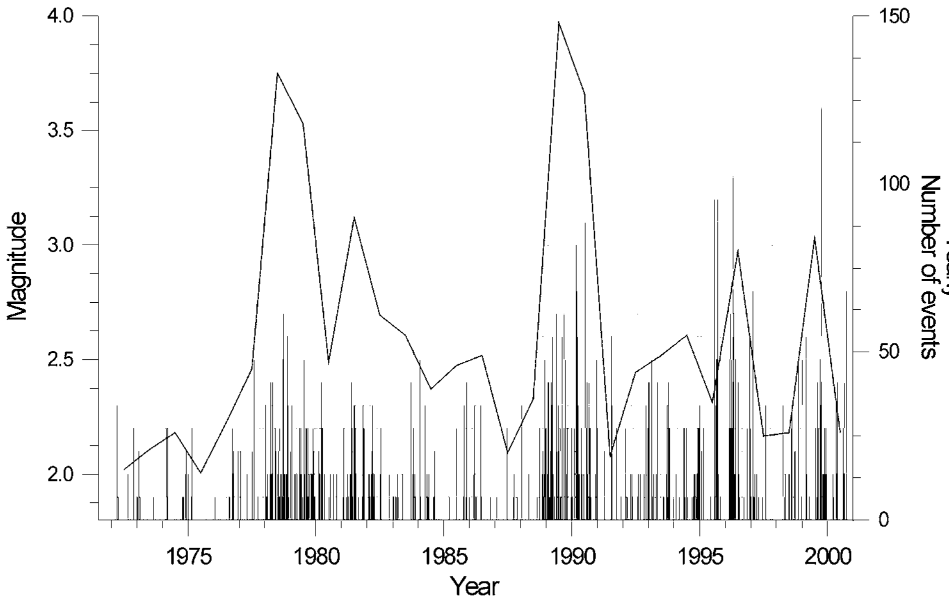

Figure 4
Time sequence of the events $M(t)$ and yearly number of earthquakes (non-overlapping time windows) with $M \geq M_{\min} = 1.8$ reported in the OV2 catalogue, from 1972 to 2000.

evidenced in these time sequences. A high number of earthquakes, however, is not necessarily associated with high magnitudes; for example, the seismic swarm in the period 1978–1980 is characterised only by moderate events ($M < 3.0$), while the largest earthquake ($M_d = 3.6$), which occurred in October 1999, is accompanied by a relatively small number of events with $M \geq M_{\min} = 1.8$.

The seismic energy release is then studied considering the quantity E^*, computed from magnitude according to the formula:

$$E^* = 10^{d(M - M_{\min})} \quad d = \text{const.} \tag{1}$$

E^* represents the energy release normalised to the energy of the minimum magnitude event considered in the analysis, that is $M_{\min} = M_{\text{completeness}} = 1.8$:

$$E^* = \frac{E}{E_{\min}} = \frac{10^{c+dM}}{10^{c+dM_{\min}}} \quad c, d = \text{const.} \tag{2}$$

The considered relationship between the energy E and the magnitude M has the classical form proposed by GUTENBERG and RICHTER (1956). The use of the normalised energy E^* allows us to make the analysis less sensitive to the choice of the empirical parameters c and d of the energy-magnitude relation, since only the coefficient d is required. In this study, to be conservative in outlining the trend of the energy release rate, we use the value $d = 1.5$, given by GUTENBERG and RICHTER (1956) for M_s, even if larger values ($d \approx 2 - 3$) are consistent with M_L (KANAMORI *et al.*,1993) or M_d (PANZA and PROZOROV, 1991) estimates.

Figure 5 shows the curve of the monthly energy release $E^*(t)$ as a function of time. The energy release exhibits a mostly constant background rate ($E^*_{\text{monthly}} \leq 50$ during about 90% of the period of observation), with sporadic periods of strongly increased rates. The periods of increased energy release are approximately: 1978–1980, 1989–1990, 1995–1996 and 1999–2000. Such anomalous time intervals are characterised (except the first one) by the occurrence of the largest magnitude events. The maximum magnitude and the average energy rate progressively increase with time, while the time intervals between subsequent periods of intense seismicity seem to decrease.

An important step towards the understanding of the time evolution of seismicity can be made by computing the time dependence of the b value in the Gutenberg-Richter (GR) relation (GUTENBERG and RICHTER, 1944; 1956). The rough estimation of the variation in time of the b value in the GR law has been performed, in moving windows containing 100 earthquakes each, shifted by 10 events, using the maximum likelihood method (WIEMER and ZUNIGA, 1994). Until 1986 b smoothly oscillates around the value 1.8; from 1988 to 1996, b is around 1.3; finally since 1996 the b value further decreases to about 1.0 (Fig. 6). The periods of most rapid change in the b value are almost the same periods in which increased energy rate and maximum magnitudes are observed.

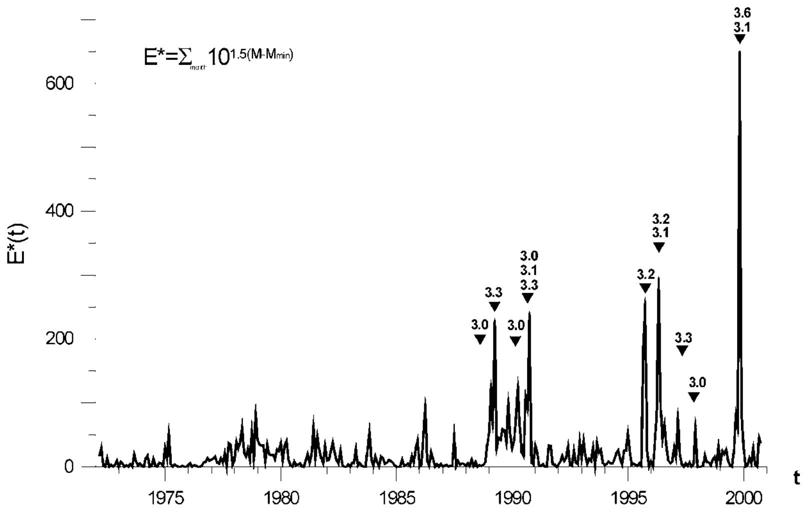

Figure 5
Diagram of the normalized monthly energy release $E^*(t)$ at Somma-Vesuvius, estimated from local earthquake magnitudes, using time windows of one month shifted by one month. Maximum magnitude event's occurrence is indicated by arrows.

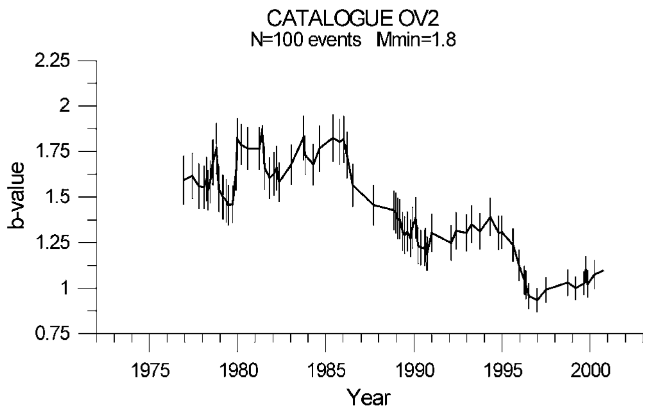

Figure 6
Time variation of the b value, estimated using the maximum likelihood method (Wiemer and Zuniga, 1994) considering groups of 100 events, shifted by 10 events; the vertical bars indicate the errors.

For the complete catalogue, we attempt to define in a unequivocally formal way the periods of "quiescence", q, characterised by some typical background seismicity, and the periods of "activity", a, where the energy release is unusually large. With this purpose we compute $E^*(t)$, grouping the events into time windows of one year, shifted by one month, and we consider the distribution of the estimated yearly energy $E^*_{\text{yearly}}(t)$, both in the cumulative and discrete form (Fig. 7). From Figure 7 we can

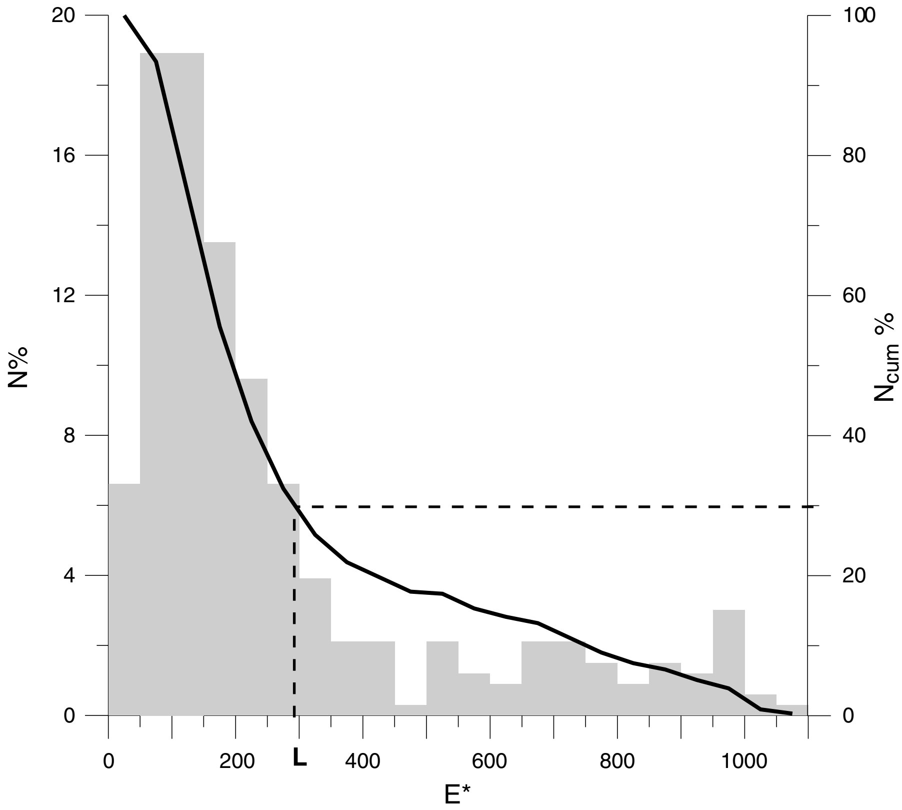

Figure 7
Distribution of the yearly energy release $E^*(t)$, estimated for $M \geq 1.8$ using time windows of one year, shifted by one month. The histogram shows the discrete distribution, the bold line, and the cumulative one. The dotted line indicates the selected threshold $L = 300$, corresponding to 30% of the time intervals.

observe that during most of the time the energy release is contained within a relatively narrow range $50 \leq E^* \leq 300$, and that the energy distribution exhibits a tail extending to quite high values of E^*. Therefore we choose the threshold $L = E^* = 300$, which selects about 30% of the considered time, practically, i.e., during 30% of the period of observation $E^*(t) \geq L = 300$ (see the cumulative distribution in Fig. 7).

The periods of activity are then defined as the time intervals within which the normalised energy release $E^*(t)$ exceeds the threshold L; in Figure 8a the intervals of quiescence and activity are indicated with q1, q2, q3, q4, q5 and a1, a2, a3, a4, respectively (Table 1).

For all the periods identified, as well as for some groups of them, the parameters a and b of the GR law are computed using the maximum likelihood method proposed by Molchan and Podgaetskaya (1973), and described in detail in Molchan *et al.*

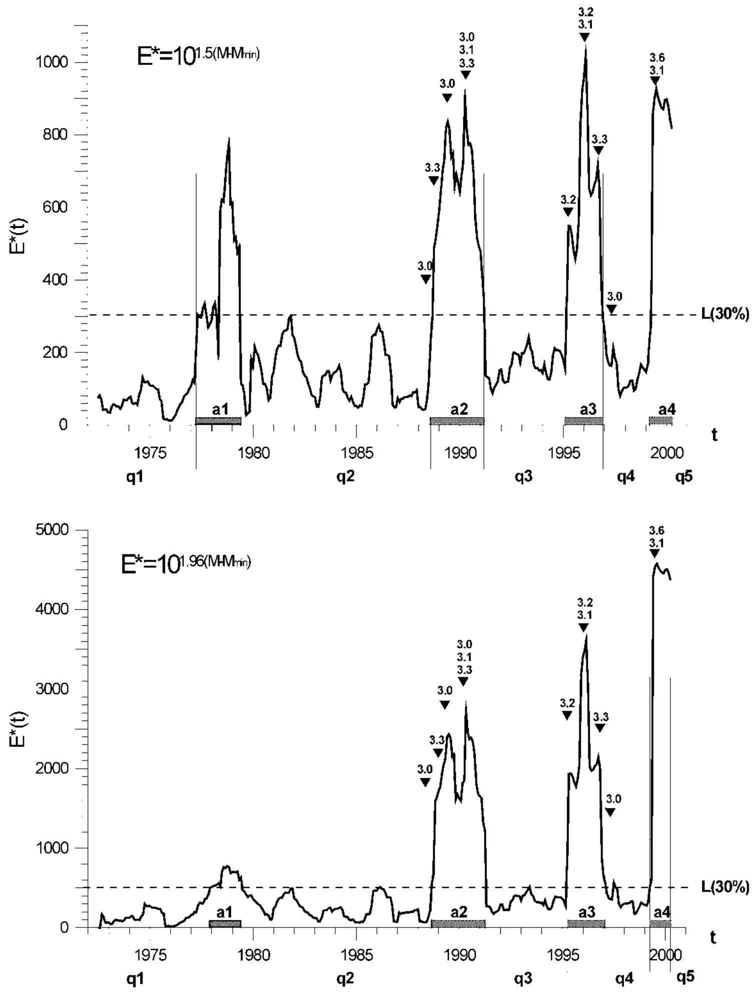

Figure 8

a) $E^*(t)$ determined for events with $M \geq 1.8$ using time windows of one year, shifted by one month, and with $d = 1.5$ (GUTENBERG and RICHTER, 1956). The triangles point to the occurrence of strong events. The grey boxes evidence the periods of activity above the threshold L (a1, a2, a3 and a4), which is indicated by the dotted line. b) The same as Figure 8a, but with $E^*(t)$ estimated considering $d = 1.96$ (KANAMORI *et al.*, 1993).

(1997). A confidence level of 95% is considered for the parameter b, and of 99% for the parameter a, assuming as minimum magnitude cut-off $M_d = 1.8$. The results, summarised in Table 2, confirm in a quantitative way the general trend shown in Figure 6.

The parameters of the GR law obtained for the different time intervals are then compared, both considering individual intervals and composite intervals, the latter being obtained merging the individual samples. The results of the

Table 1

Time intervals (initial and final time) and point estimates of the parameters a,b of the GR law for the different intervals of quiescence and activity, as shown in Figure 8a. N is the number of events within each time window

Interval	Time window	b value		N
		a-intervals	q-intervals	
q1	1972.2.23–1977.10.31		1.59	143
a1	1977.11.1–1979.5.31	1.56		190
q2	1979.6.1–1988.7.31		1.72	482
a2	1988.8.1–1991.2.28	1.32		307
q3	1991.3.2–1995.1.31		1.29	167
a3	1995.2.1–1996.12.1	0.90		107
q4	1996.12.2–1999.2.28		1.08	62
a4	1999.3.1–2000.4.1	1.04		83
q5	2000.4.2–2000.10.9		1.05	21

Table 2

Estimates of the parameters a,b of the GR law for the individual and composite time intervals. N is the number of events within each time window. [$b_{\min}$, $b_{\max}$] indicates the 95% confidence level interval for the parameter b. The value of a is normalised for a time interval of one year, for an area of 1000 km^2 and for a reference magnitude $M_0 = 2$ (MOLCHAN et al., 1997)

Interval		$P_b = 95\%$			P_a 99%	
	N	b	$b_{\min}$	$b_{\max}$	a	Δa
a1	190	1.56	1.34	1.80	2.24	0.165
a2	307	1.32	1.17	1.47	2.22	0.129
a3	107	0.90	0.72	1.11	1.86	0.221
a4	83	1.04	0.81	1.30	2.00	0.251
q1	143	1.59	1.33	1.88	1.56	0.190
q2	482	1.72	1.56	1.88	1.87	0.103
q3	167	1.29	1.09	1.50	1.78	0.176
q4	62	1.08	0.80	1.38	1.56	0.292
q5	21	1.05	0.60	1.59	1.72	0.512
a1 + a2	497	1.40	1.28	1.53	2.32	0.101
a3 + a4	190	0.96	0.81	1.12	1.92	0.165
q1 + q2	625	1.69	1.55	1.83	1.79	0.090
q3 + q4 + q5	250	1.21	1.05	1.37	1.71	0.143
(a1 + a2) + (q1 + q2)	1122	1.53	1.45	1.64	1.93	0.067
(a3 + a4) + (q3 + q4 + q5)	440	1.09	0.98	1.20	1.79	0.108

comparison of the b value for individual intervals are presented in Table 3, while the results of the comparison of the parameters a, b for composite groups of data are shown in Table 4.

The choice of the threshold L is rather arbitrary, however several tests made changing the threshold within reasonable intervals, show that the definition of

Table 3

Comparison of the parameter b of the GR law for the different intervals identified in Figure 8a. Nf is the number of degrees of freedom. The b values differ with a significance level of 95%, if the probability π is larger than 95%

Intervals compared	Test/Nf	π %	Conclusion of the comparison
a1, a2, a3, a4	21.8/3	> 99.95	*b* values are different
a1, a2	3.1/1	92.6%	the difference in *b* values is not significant
a3, a4	0.7/1	61.0%	the difference in *b* values is not significant
q1, q2, q3, q4, q5	21.5/4	> 99.95	*b* values are different
q1, q2	0.6/1	55.0%	the difference in *b* values is not significant
q3, q4, q5	1.7/2	58%	the difference in *b* values is not significant

Table 4

Comparison of the parameters a,b of the GR law for the different composite time intervals of activity and quiescence. Nf is the number of degrees of freedom. The b values differ with a significance level of 95%, if the probability π is larger than 95%

Composite samples	N	b	$b_{\min}$	$b_{\max}$	a	Δa	Test/Nf*	π %	Conclusion
a1 + a2	497	1.37	1.26	1.49	2.20	.095	17.91/1	> 99.95	*b* values are different
a3 + a4	190	0.96	0.81	1.12	1.92	.165			
q1 + q2	625	1.69	1.55	1.84	1.77	.096	19.17/1	> 99.95	*b* values are different
q3 + q4 + q5	250	1.21	1.05	1.37	1.71	.143			
a1 + a2 + q1 + q2	1122	1.51	1.42	1.61	1.93	.067	36.69/1	> 99.95	*b* values are different
a3 + a4 + q3 + q4 + q5	440	1.09	.98	1.20	1.79	.108			

quiescence and activity periods varies only moderately, and consequently the values of a and b are quite stable.

Finally, in order to verify the stability of the results with respect to the choice of the coefficient d in the equation (1), the analysis has been repeated considering a different energy-magnitude relation. We consider, for example, the value $d = 1.96$ proposed by KANAMORI *et al.* (1993) to compute the quantity $E^*(t)$ and the corresponding threshold L (Fig. 8b). Comparing Figures 8a and 8b, it is possible to observe that the time intervals of activity and quiescence thus identified do not differ significantly, the main variation being a larger increasing trend of the energy release rate in Figure 8b.

The seismicity does not appear as a periodic expression of a repetitive underlying process, rather it seems to evolve with periods of intense activity (1989; 1995–1996; 1999). The decrement of the b value (Fig. 6) indicates the increase with increasing time of the rate of the large events, in agreement with the progressive growth, from 1988 to 1999, of the maximum observed magnitude (from 3.2 to 3.6). The first decrease of b occurs just before the crisis of 1989. The parameters estimated for the intervals of quiescence and activity (Tables 1 and 2), confirm the general decrement of the b value with increasing time. The two GR laws obtained for the time periods [a1 + a2 + q1 + q2] ($b = 1.51 \pm 0.09$) and [a3 + a4 + q3 + q4 + q5] ($b = 1.09 \pm 0.11$), that is before and after February 1991, differ with a confidence level of 99.95%.

Earthquake Source Processes

We study the earthquake sources of the largest events with two different approaches. The first (method 1), originally developed by BRUNE (1970), permits the estimation of the scalar seismic moment M_0 from the amplitude, at low frequency, of the displacement spectra in the assumption that the source mechanism can be satisfactorily represented by a double-couple; the second (method 2), based on the waveform inversion, retrieves the full seismic moment tensor without any *a priori* constraints on the source mechanism. Indeed the seismic moment tensor can be decomposed into double-couple (DC), compensated linear vector dipole (CLVD) and volumetric (V) components, and it is very suitable to investigate the physical changes within a volcano, related to magma or fluid movements (e.g., KNOPOFF and RANDALL, 1970; JOST and HERRMANN, 1989).

To determine the full seismic moment tensor we apply the method developed by SILENY *et al.* (1992), SILENY (1998). The method, already applied in volcanic areas (e.g., CAMPUS *et al.*, 1993; SARAÒ *et al.*, 2001), works in the point source approximation and consists of two main steps: 1) unconstrained linear inversion to retrieve, from the recorded seismograms, the six moment rate functions (MTRF) and 2) constrained nonlinear inversion where the MTRF's are used as data to obtain the focal mechanism, the scalar seismic moment and the source time function. In the *first step* the moment rate functions are obtained by deconvolution of the Green's functions from the data. The synthetic Green's functions are computed by modal-summation technique (e.g., PANZA, 1985; FLORSCH *et al.*, 1991; PANZA *et al.*, 2001) for a grid defined by a range of hypocentral coordinates and by two structural models assumed to be representative of the model space around the source and the recording station. At a generic point within the space where the grid is defined, the Green's function is determined by interpolating the Green's functions computed, for the two structural models, at nearby grid points. Once the Green's functions are determined, the MTRFs are obtained applying a method based on SIPKIN (1982) approach to obtain reliable moment rate functions when processing local high-frequency waveforms, and by using a parameterisation of the moment rate functions by a series of triangles overlapping in their half-width (NABELEK, 1984). With the retrieved MTRFs, synthetic seismograms are computed and compared with the observed ones. The L_2 norm of their residuals is minimized by an iterative process that singles out the minimum corresponding to the best MTRFs which can be considered as solution of the first step.

In the second step, assuming that for a weak event it is reasonable to expect a constant mechanism during the energy release, we search for their correlated part. The problem is nonlinear and it is solved iteratively by imposing constraints such as positivity of the source time function and the requirement that the equal polarity areas are distributed consistently with clear readings of first arrival polarities, when these are available. The mechanism and the source time function are obtained after factorization of the MTRFs. The factorization of the MTRFs reduces the bias due to the modelling of the Green's function since it works only on their coherent part. The predicted MTRFs are then matched to the observed MTRFs obtained as output of the first step.

The advantage of this approach is a simplification of the problem of fitting the input seismograms by converting it into a problem of matching the MTRFs. The number of MTRFs is fixed at six, or five when dealing with only deviatoric sources, and their length is controlled by the number of triangles used for their parameterization. Considering the MTRFs as an independent function in step 1 leads to an overparameterization of the problem which is advantageous to absorb inadequate modeling of the structure (KRAVANJA *et al.*, 1999). The effects due to local heterogeneities and to wave propagation, such as attenuation, reflection or scattering, are in this way reduced. The effects of inadequacies of the structural models have been investigated by SILENY *et al.* (1992), KRAVANJA *et al.* (1999). Starting from a double-couple mechanism with an instantaneous source time function they proved, by synthetic tests, that a poorly known structure, not contained in the allowed interpolation range of the Green's functions (1) causes mainly the presence of apparent non-double-couple components in the moment tensor solutions and contaminates particularly the CLVD that increases from 0% of the starting model to 40% for large inconsistency cases; (2) does not affect the orientation of the double-couple that remains stable within $\pm$ 10°, and (3) leads to spurious peaks in the source time function (KRAVANJA *et al.*, 1999). Mislocation of the hypocentre and the use of an inadequate model of the medium may enlarge the error bars of the source time function by about 20%. Nevertheless, when introducing the variance due to the noise present in the data and to the modelling of the Green's functions, the error analysis (SILENY *et al.*, 1996; SILENY, 1998) indicates the level of reliability of the solutions (PANZA and SARAÒ, 2000). On the other hand if the percentage of non-double-couple components can be affected by systematic errors due to poor structural modeling, when looking at data sharing similar paths in the same area, their variation and the observed trend are free from such a shortcoming (SARAÒ *et al.*, 2001).

Tests done on synthetic data have also shown that the inversion results are stable until the noise in the data is less than 20% of the maximum amplitude (SILENY *et al.*, 1996; CESPUGLIO *et al.*, 1996). The solutions are stable even when few stations are used (SILENY *et al.*, 1992). Indeed for the determination of the six independent components of the moment tensor in time domain, the six independent data are obtained from *P*, *SV* and *SH* arrivals at two stations (e.g., STUMP and JOHNSON, 1977; PANZA and SARAÒ, 2000) and two three-component stations or three vertical component stations, are mathematically sufficient, to solve the moment tensor components.

Data Analysis and Results

From the seismicity which occurred at Mt. Vesuvius during the period 1989–1997 we studied six events, located in the central part of the volcano, with duration magnitude greater or equal to 3.0 (Table 5) for which digital waveforms were available. Noisy seismograms, or data for which the epicentral distance was too small compared with the hypocentral depth computed by standard routine (HYPO71) are not included. The latter condition is necessary for a straightforward application of the modal-summation technique when computing the Green's function. A minimum of four signals, depending on the quality of the data, is required for each inversion. The recording stations (Fig. 1) are run by Osservatorio Vesuviano and are equipped with geophones Mark L4-3-D with natural period of 1 s. The velocities, recorded at a sampling frequency of 125 Hz, have been resampled at 20 Hz. On the basis of several tests to guarantee clear arrivals and high signal-noise ratios, as a rule, we low-pass filter seismograms at 5 Hz using a gaussian filter. After mean removing, tapering and filtering, we select the temporal window of the seismograms to be inverted.

For the waveform inversion the Green's functions are computed employing different structural models for each path source-station and for the source area that practically coincides with the center of the volcano. Each structure is adjusted from the 3-D velocity model proposed by DE NATALE *et al.* (1998) and from the attenuation values reported in BIANCO *et al.* (1999). The density values are computed using the empirical Nafe-Drake curves.

Table 5

The focal depth is referred to 0.9 km above the sea level. M_0 is the scalar seismic moment computed by Brune approach (method 1) and by moment tensor analysis (method 2)

N.	Date	Focal depth (km)	M_d	Method 1 $M_0 \times 10^{13}$ Nm	Method 2 $M_0 \times 10^{13}$ Nm
1	19.3.1989	1.6	3.3	5.8 ± 3.1	1.4 ± 0.6
2	24.9.1995	2.4	3.1	3.1 ± 0.6	1.4 ± 0.4
3	25.4.1996	3.5	3.3	2.4 ± 0.7	4.8 ± 0.3
4	5.11.1997	3.2	3.0	2.0 ± 1.0	1.0 ± 0.3
5	9.10.1999	3.9	3.6	11.1 ± 5.0	6.6 ± 1.1
6	11.10.1999	2.8	3.1	1.9 ± 0.8	2.2 ± 0.1

To reduce the number of unknowns and to make more stable the results of the inversions, we fix the epicentre—the best constrained parameter by routine locations—of the studied events to the values computed by OV and we invert only for the hypocentral depth and the six components of the moment tensor. The damping value used in the inversion has been selected, after several tests, equal to 10^{-2} to minimize the spurious non-DC components.

Whenever possible, inversions for the same event considering either different sets of records or introducing a kinematical correction for the station elevation have been performed to test the stability of the results. Moreover since spurious non-double couple components can arise only resulting from the station configuration (PANZA and SARAÒ, 2000), we performed synthetic tests to define lower limits above which the non-double couple components found can be considered statistically significant. The main results obtained for the six studied earthquakes are reported in Table 5.

In Figure 9 the results of the waveform inversion are given. The fit of the data against synthetic signals is reported for all the studied events. The common feature to most of the studied events is the existence of a relevant V component (Fig. 10) that is consistent with the presence of magmatic degassing processes and of superheating of the water-bearing stratum. The presence of a V component in the 1996, April 25 event, was estimated by the independent analysis of VILARDO (1996).

The comparison with the Etna seismicity studied by SARAÒ *et al.* (2001) shows that the V component is more relevant for the Vesuvius events.

Discussion and Conclusions

DE NATALE *et al.* (2000) showed that the local seismicity at Somma-Vesuvius is strongly clustered around the crater axis, i.e., within less than 1 km from the crater centre, in the depth range 0–6 km. A certain level of background activity is always present at this volcano. Despite the overall constancy of the seismically active volume, we have shown that time and energy distribution of the events does not appear constant in the last three decades. DE NATALE *et al.* (2000) interpreted the seismic background mainly in terms of local gravitative loading of the volcanic edifice, focused around the crater axis by a marked rigidity anomaly. The accurate analyses of the seismic catalogue presented in this paper, however, show that seismicity cannot be entirely considered as a simple background activity with constant properties. In fact, it consists of periods of alternating low and high seismicity levels. The curve of the monthly energy release, computed along the three decades spanned by the catalogue, shows clearly that the low seismicity levels are characterised by an energy rate with features rather uniform in time. Such a rate of energy release during low activity periods can be considered representative of the background seismic level. Superimposed to such background activity, intense seismicity episodes occasionally occur. Differently from those of low seismicity,

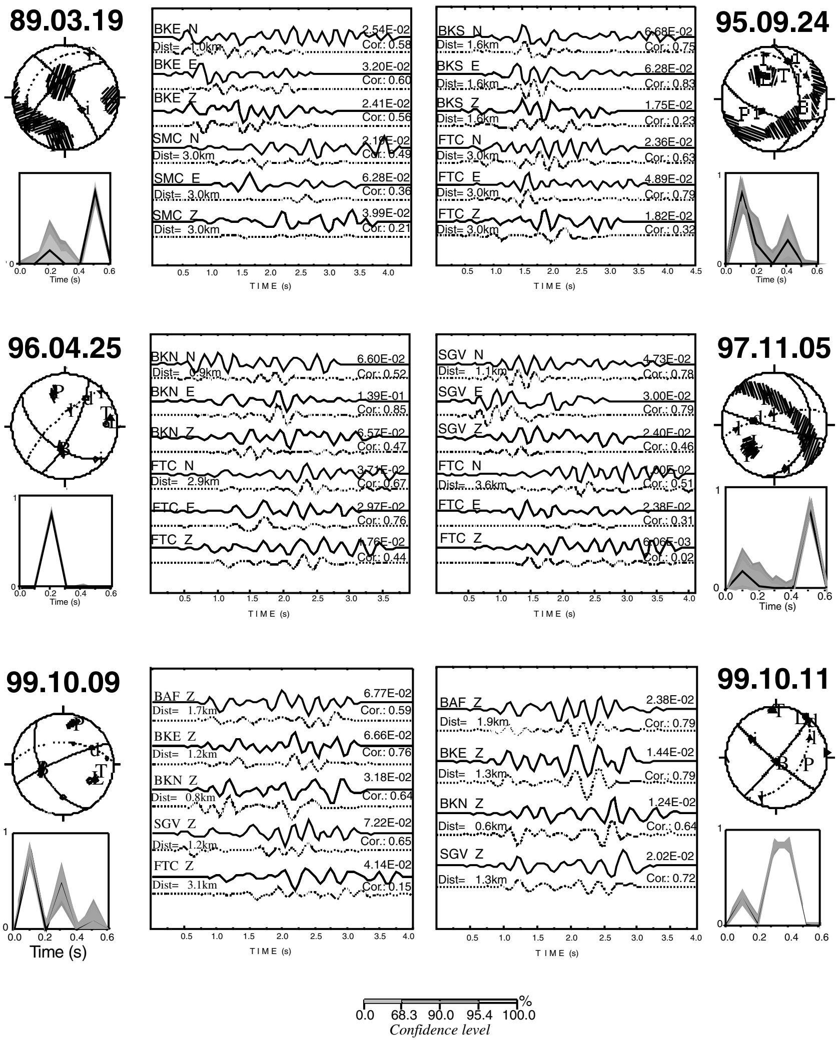

Figure 9

Results from the waveform inversion of the events listed in Table 5. — Real data (solid line) and synthetic signals (dotted line): the epicentral distances, the station name and the component used are reported on the left of the panel, whereas the maximum amplitudes and the correlation values are reported on the right. — Focal mechanism with confidence error ellipses in the RIEDESEL-JORDAN (1989) representation: L is the vector describing the total mechanism, d is the DC vector, l and l' are the CLVD with major dipole along the tensional and the pressure axes respectively, i represents V. T, P and B indicate the tensional, compression and null axes respectively. The dashed line represents the locus of the deviatoric mechanism. Hatched areas around the L, P, T, B axes are the projections of the 97% confidence ellipses onto the focal sphere. The distance of L from the vectors i, d, l, and l' displays the share of V, DC and CLVD part that can be considered reliable. – Source time function: the error bars are plotted with a grey scale according to different values of confidence.

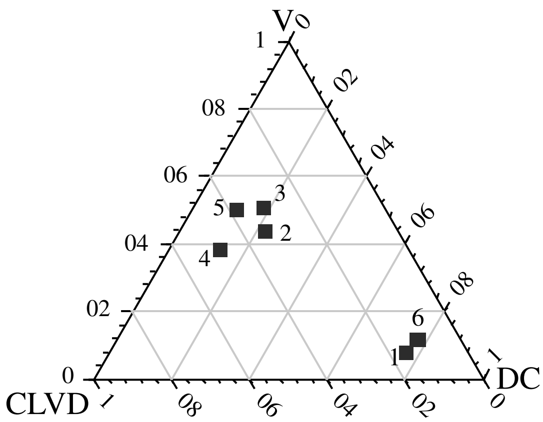

Figure 10
Triangular representation of the moment tensor components for the earthquakes numbered as in Table 5.

high seismicity periods are characterised by energy rates with a clearly increasing trend in time. The first period of increased seismicity is observed around 1977–1980. The average rate of energy release in such a period increases to a value of about 0.3×10^{10} J/month, with respect to the background level which is below 0.1×10^{10} J/month. The second period of seismic crisis occurs in 1989–1990. The energy release rate in this period is of about 0.8×10^{10} J/month, higher than in 1977–1980. In 1989 the first earthquakes with magnitude above 3 appear in the Vesuvius seismic sequence and some years before the 1989 crisis, around 1986, the *b* value of the sequence changes significantly, from 1.7–1.8, characteristic of the 1972–1986 period, to a lower value (1.3). Such a *b* value remains practically constant until the subsequent crisis of 1995–1996, when it further decreases, to 1.0, a value that persists until the end of the available to us observations (October, 2000). The evidence that the *b*-value can significantly decrease in volcanic areas, as a consequence of the fracture coalescence generating progressively larger faults, is supported by recent studies and laboratory experiments (MEREDITH *et al.* 1990). The observed decrease of *b* is particularly relevant if we consider the recent results obtained by ESPOSITO *et al.* (2000) who estimated a *b* value ranging between 0.75 and 1.05 in the seismic crises associated with past Vesuvius eruptions.

The crisis of 1995–1996 is characterised by a larger energy rate, with respect to the 1989–1990 period (about 0.9×10^{10} J/month). The last crisis, spanning the end of 1999-beginning of 2000, is characterised by an even higher energy rate, of about 2.0×10^{10} J/month. The maximum earthquake magnitudes during periods of crisis increase with time, from the values $M_d < 3.0$ of 1977–1978 to $M_d = 3.2$ of 1989–1990, $M_d = 3.4$ in 1996 and $M_d = 3.6$ in October 1999. The change in the maximum magnitude of each active period is consistent with the progressive increase of the *b* value. Furthermore, the *b* values, whose rapid changes roughly correspond with periods of crisis, remain constant after the end of each crisis. This progressive escalation of energy release and of the maximum magnitudes during periods of intense activity indicates that the energy involved in the process increases with time and that some peculiar dynamic processes are superimposed to the constant background. A very important point evidenced in this paper is that the seismic sequence exhibits an internal dynamic, pointing towards progressively higher energy rates, and not a repetitive character as would be expected for a simple background activity. From all the existing literature, based on historical observations of pre-eruptive periods, no clear evidence exists for events with magnitudes larger than 4, except perhaps the earthquake which occurred in 62 A.D., 17 years before the 79 plinian eruption. Moreover, no evidence exists for very intense seismicity before large eruptions, so that the period preceding the next eruption also could be characterized by seismic sequences very similar, in number and magnitude, to those observed during recent periods of crisis. Another key point for the evaluation of the eruptive hazard in this area is the careful estimation of the earthquake source properties necessary to understand the nature of the seismicity during the critical periods. The apparent features of most of the observed earthquakes are those normally associated with volcano-tectonic events. However, the reliable determination of the source moment tensor of the most energetic events ($M_d > 3.0$) evidences the presence, in the seismic source, of strong isotropic components, which in most cases indicates explosion. Such isotropic components are statistically significant, at more than 95% significance level, for most of the analysed events, and are in agreement with the observations of low S/P amplitude ratios, as compared with those theoretically expected from the best double couple mechanisms.

The seismicity of Mt. Vesuvius in the last three decades appears to comprise the superposition of a background level and of sporadic periods of intense activity. The genesis of the largest earthquakes occurring during the intense seismicity episodes is likely to involve internal dynamics, linked perhaps to magma movements or to volatile exolution, as indicated by the strong isotropic components, consistent with explosive processes. The inferred non double-couple components, in fact, indicating explosion, are considerably different from those inferred at Mt. Etna (SARAÒ *et al.*, 2001). Such a difference possibly reflects the different magmatic properties of the two areas. At Mt. Etna, where magmas are deficient in volatiles, non double-couple components basically indicate CLVD, i.e., a kind of compensated tensile cracks. At Mt. Vesuvius, where magmas are rich in volatiles generating explosive mixtures, the largest earthquakes are characterised by relevant explosive components in the moment tensor.

In conclusion, even if the common background seismic activity at Somma-Vesuvius, volcano-tectonic in character, does not generate particular concern, sporadic high seismicity episodes must be accurately monitored and evaluated. At the moment, it is not yet possible to uniquely interpret such episodes, nonetheless they may indicate the presence of an ongoing internal volcanic activity, superimposed to that one generating the ordinary background seismicity.

Acknowledgements

We thank U. Coppa for providing the digital data of the 1989 crisis and for useful suggestions pertaining to the 1999 crisis. We acknowledge the anonymous referee whose criticism enhanced the manuscript. This study was partially supported by the Italian CNR-GNV (grant 98.00695.PF62), by INGV funds ''Eruptive Scenarios from Physical Modeling and Experimental Volcanology'' and by EU VOLCALERT project.

REFERENCES

BERRINO, G., COPPA, U., DE NATALE, G., and PINGUE, F. (1993), *Recent geophysical investigation at Somma-Vesuvio volcanic complex*. In *Mount Vesuvius* (De Vivo B., Scandone R., and Trigila R., editors), J. Volcanology and Geothermal Research *58*, 239–262.

BIANCO, F., CASTELLANO, M., DEL PEZZO, E., and IBANEZ, J. M. (1999), *Attenuation of Short-period Seismic Waves at Mt. Vesuvius, Italy*, Geophys. J. Int. *138*, 67–76.

BRUNE, J. N. (1970), *Tectonic Stress and the Spectra of Seismic Shear Waves from Earthquakes*, J. Geophys. Res. *75*, 4997–5009.

CAMPUS, P., CESPUGLIO, G., and PANZA, G. F. (1993), *Atti dell'Accademia dei Lincei relativi a International Conference Large explosive eruptions (The Problem of Eruptions, Forecasting Full Moment Tensor Retrieval and Fluid Dynamics in Volcanic Areas: The Case of Plegrean Fields (South Italy), and Warning; Limits and Possibilities)*, 81–101.

CAPUANO, P., COPPA, U., DE NATALE, G., DI SENA, F., GODANO, C., and TROISE, C. (1999), *A detailed analysis of some local earthquakes at Somma-Vesuvius*. In *Physics of volcanic phenomena and eruption precursors* (De Natale G., Gasparini P., Coppa U., editors), Annali di Geofisica *42* (3), 391–405.

CESPUGLIO, G., CAMPUS, P., and SILENY, J. (1996), *Seismic Moment Tensor Resolution by Waveform Inversion of a Few Local Noisy Records-II. Application to Phlaegrean Fields (Southern Italy) Volcanic Tremors*, Geophys. J. Int. *126*, 620–634.

DEL PEZZO, E., IANNACCONE, G., MATINI, M., and SCARPA, R. (1983), *The 23 November 1980 Southern Italy earthquake*, Bull. Seismol. Soc. Am. *1*, 187–200.

DE NATALE, G., CAPUANO, P., TROISE, C., and ZOLLO, A. (1998), *Seismicity at Somma-Vesuvius and its Implication for the 3-D Tomography of the Volcano*, J. Volcanol. Geotherm. Res. *82*, 175–197.

DE NATALE, G., PETRAZZUOLI, S. M., TROISE, C., PINGUE, F., and CAPUANO, P. (2000), *Internal Stress at Mt. Vesuvius: A Model for Background Seismicity at Central Volcano*, Geophys. Res. *105* (B7), 16,207–16,214.

ESPOSITO, E., MASTROLORENZO, G., and PORFIDO, S. (2000), *Seismicity at Vesuvius, a Comparison between Historical Eruptive Periods and Present Time*. Abstract. EGS 2000. Nizza, France.

FLORSCH, N., FÄH, D., SUHADOLC, P., and PANZA, G. F. (1991), *Complete Synthetic Seismograms for High-Frequency Multimode SH-waves*, Pure Appl. Geophys. *136*, 529–560.

GUTENBERG, B. and RICHTER, C. F. (1944), *Frequency of Earthquakes in California*, Bull. Seismol. Soc. Am. *34*, 185–188.

GUTENBERG, B. and RICHTER, C. F. (1956), *The energy of earthquakes*. Q. J. Geol. Soc. London, *112*, 1–14.

IANNACCONE, G., ALESSIO, G., BORRIELLO, G., CUSANO, P., PETROSINO, S., RICCIOLINO, P., TALARICO, G., and TORELLO, V. (2001), *Characteristics of the Seismicity of Vesuvius and Campi Flegrei during the year 2000*, Annali di Geofisica *44* (5/6), 1075–1091.

JOST, M. L. and HERRMANN, R. B. (1989), *A Student's Guide to and Review of Moment Tensors*, Seismol. Res. Lett. *60*, 37–57.

KANAMORI, H., MORI, J., HAUKSSON, E., HEATON, TH., HUTTON, L. K., and JONES, L. M. (1993), *Determination of Earthquake Energy Release and ML Using TERRASCOPE*, Bull. Seismol. Soc. Am. *83*, 2, 330–346.

KNOPOFF, L. and RANDALL M. (1970), *The Compensated Linear-vector Dipole: A Possible Mechanism for Deep Earthquakes*, J. Geophys. Res. *75*, 4957–4963.

KRAVANJA, S., PANZA, G. F., and SILENY, J. (1999), *Robust Retrieval of a Seismic Point-source Time Function*, Geophys. J. Int. *136*, 385–394.

MARTURANO, A. and RINALDIS, V. (1995), *Archeaologie und Seismology* (Verlag Biering and Brinkmann, München) pp. 131–135.

MARTURANO, A. and RINALDIS, V. (1996), *Seismic History and Consistent Seismicity; Evidence from Southern Italy*, Natural Hazards *14*, 11–21.

MARZOCCHI, W., VILARDO, G., HILL, D. P., RICCIARDI, G. P., and RICCO, C. (2001), *Common Features and Peculiarities of the Seismic Activity at Phlegraean Fields, Long Valley, and Vesuvius*. Bull. Seismol. Soc. Am. *91*, 191–205.

MEREDITH, P. G., MAIN, I. G. and JONES C. (1990), *Temporal variations in seismicity during quasi-static and dynamic rock failure*, Tectonophysics, *175*, 249–268.

MOLCHAN, G. M. and PODGAETSKAYA, V. M. (1973), *Parameters of global seismicity*. In (*V. I. Keilis-Borok, ed.*), *Comput. Seismology*; *6*, Nauka, Moscow, 44–66 (in Russian).

MOLCHAN, G., KRONROD, T., and PANZA, G. F. (1997), *Multi-scale Seismicity Model for Seismic Risk*, Bull. Seismol. Soc. Am. *87*, 1220–1229.

NABELEK, J. L. (1984), *Determination of Earthquake Source Parameters from Inversion of Body Waves*, Ph.D. Thesis, Massachusetts Institute of Technology, Cambridge, USA.

PANZA, G. F. (1985), *Synthetic Seismograms: The Rayleigh Waves Modal Summation*, J. Geophys. *58*, 125–145.

PANZA, G. F. and PROZOROV, A. (1991), *High Frequency Seismic Sources Characterize the Areas of Tectonic Shortening in the Italian Region*, Rend. Fis. Acc. Lincei *2*, 107–116.

PANZA, G. F. and SARAÒ, A. (2000), *Monitoring Volcanic and Geothermal Areas by Full Seismic Moment Tensor Inversion: Are Non-double Couple Components Always Artefacts of Modeling?* Geophys. J. Int. *143*, 353–364.

PANZA, G. F., ROMANELLI, F., and VACCARI, F. (2001), *Seismic Wave Propagation in Laterally Heterogeneous Anelastic Media: Theory and Applications to Seismic Zonation*, Advances in Geophysics *43*, 1–95.

RIEDESEL, M. A. and JORDAN, T. H. (1989), *Display and Assessment of Seismic Moment Tensors*, Bull. Seismol. Soc. Am. *79*, 85–100.

ROLANDI, G., BARRELLA, A. M., and BORRELLI, A. (1993), *The 1631 Eruption of Vesuvius*, Volcanol. Geotherm. Res. *58*, 183–201.

ROSI, M., PRINCIPE, C., and VECCI, R. (1993), *The 1631 Vesuvius Eruption. A Reconstruction Based on Historical and Stratigraphical Data*, J. Volcanol. Geotherm. Res. *58*, 151–182.

SANTACROCE, R. (ed.), (1987), *Somma-Vesuvius*. Quaderni dell Ricerca Scientifica, CNR Roma *114*, 1–251.

SARAÒ A., PANZA, G. F., PRIVITERA, E., and COCINA, O. (2001), *Non-double Couple Mechanisms in the Seismicity Preceeding 1991–1993 Etna Volcano Eruption*, Geophys. J. Int. *145*, 319–335.

SCANDONE, R., GIACOMELLI, L., and GASPARINI (1993), *Mount Vesuvius: 2000 Years of Volcanological Observations*, J. Volcanol. Geotherm. Res. *58*, 5–25.

SIGURDSSON, H., CAREY, S., CORNELL, W., and PESCATORE, T. (1985), *The Eruption of Vesuvius on AD 79*, Natl. Geogr. Res. *1*, 332–387.

SILENY, J., PANZA, G. F., and CAMPUS, P. (1992), *Waveform Inversion for Point Source Moment Tensor Retrieval with Optimization of Hypocentral Depth and Structural Model*, Geophys. J. Int. *108*, 259–274.

SILENY, J., CAMPUS, P., and PANZA, G. F. (1996), *Seismic Moment Tensor Resolution by Waveform Inversion of a Few Local Noisy Records—I. Synthetic Tests*. Geophys. J. Int. *126*, 605–619.

SILENY, J. (1998), *Earthquake Source Parameters and their Confidence Regions by a Genetic Algorithm with a "Memory"*, Geophys. J. Int. *134*, 228–242.

SILENY, J. and VAVRYCUK, V. (2000), *Approximate Retrieval of the Point Source in Anisotropic Media: Numerical Modelling by Indirect Parameterization of the Source*, Geophys. J. Int. *143* (3), 700–708.

SIPKIN, S. A. (1982), *Estimation of Earthquake Source Parameters by the Inversion of Waveform Data: Synthetic Waveforms*, Phys. Earth. Planet. Inter. *30*, 242–259.

STUMP, B. V. and JOHNSON, L. R. (1977), *The Determination of Source Properties by the Linear Inversion of Seismograms*, Bull. Seismol. Soc. Am. *67*, 1489–1502.

VILARDO, G. (1996), *Rapporto sismico Vesuviano del 25 April 1996*, Report Osservatorio Vesuviano, Napoli.

VILARDO, G., VENTURA, G., and MILANO, G. (1999), *Factors Controlling the Seismicity of the Somma-Vesuvius Volcanic Complex*, Volcanology and Seismology *20* (2) 219–238.

VILARDO, G., BIANCO, F., CAPELLO, M., CASTELLANO, M., and MILANO, G. (2002), *Mt Vesuvius Seismic Activity, 1996*. Acta Vulcanologica, in press.

WIEMER, S. and ZUNIGA, R. F. (1994), *ZMAP – A Software Package to Analyze Seismicity*, EOS, Transactions, Fall Meeting, AGU *75*, 456.

ZOLLO, A., GASPARINI, P., VIRIEUX, J., LE MEUR, H., DE NATALE, G., BIELLA, G., BOSCHI, E., CAPUANO, P., DE FRANCO, R., DELL'AVERSANA, P., DE MATTEIS, R., GUERRA, I., IANNACCONE, G., MIRABILE, L., and VILARDO, G. (1996), *Seismic Evidence for a Low-Velocity Zone in the Upper Crust Beneath Mount Vesuvius*, Science *274* (5287), 592–594.

(Received February 26, 2002, accepted June 28, 2002)

Diagnosis of Time of Increased Probability (TIP) for volcanic earthquakes at Mt. Vesuvius

I. Rotwain[1], G. De Natale[2], I. Kuznetsov[1], A. Peresan[3], G.F. Panza[3, 4]

[1] *International Institute for Earthquake Prediction Theory and Mathematical Geophysics, Warshavskoe sh., 79, k.2, Moscow, Russia*

[2] *Osservatorio Vesuviano- Istituto Nazionale di Geofisica e Vulcanologia, via Diocleziano 328, I-80124 Naples, Italy.*

[3] *Department of Earth Science, University of Trieste , via E. Weiss 1, 34127, Trieste, Italy*

[4] *The Abdus Salam International Centre for Theoretical Physics, SAND Group, 34100, Trieste, Miramare, Italy*

Abstract

The possibility of intermediate-term earthquake prediction at Mt. Vesuvius by means of the CN algorithm is explored. CN was originally designed to identify the Times of Increased Probability (TIPs) for the occurrence of strong tectonic earthquakes, with magnitude $M \geq M_0$, within a region a priori delimited. Here the CN algorithm is applied, for the first time, to the analysis of volcanic seismicity. The earthquakes recorded at Mt. Vesuvius, during the period from February 1972 to June 2004, are considered and the magnitude threshold M_0, selecting the events to be predicted, is varied within the range: 3.0 - 3.3. Satisfactory prediction results are obtained, by retrospective analysis, when a time scaling is introduced. In particular, when the length of the time windows is reduced by a factor 2.5 – 3, with respect to the standard version of CN algorithm, more than 90% of the events with $M \geq M_0$ occur within the TIP intervals, with TIPs occupying about 30% of the total time considered. The control experiment "Seismic History" demonstrates the stability of the obtained results and indicates that the CN algorithm can be applied to monitor the preparation of impending earthquakes with $M \geq 3.0$ at Mt. Vesuvius.

1. Introduction

Since the ancient Roman times, due to the catastrophic eruption of 79 a.d., Mt. Vesuvius is probably the most known volcano all over the World. Actually, it is the volcano with the highest associated risk, because of the high explosivity of potential eruptions and the very large urban development of the area, which includes about 700,000 people living within 10 km from the main crater and the city of Naples (2 million people) twice the distance. After the last eruption, which occurred in 1944, the volcano is in a quiescent stage, with the most prominent signal of internal dynamics represented by the occurrence of local volcano-tectonic seismicity. This seismicity involves earthquakes with maximum magnitude M_d = 3.6, occurring in a shallow depth range between the top of volcano and 5 km b.s.l. (*Vilardo et al.,* 1996; *De Natale et al.,* 1998; *De Natale et al.,* 2000). *De Natale et al.* (2000) modeled the background level of seismicity as mainly due to the local gravitational stress caused by the volcano edifice loading, with the concurrent effect of regional stress changes. *De Natale et al.* (2004) recognized that, superimposed to a mean background level, occasional intense peaks of seismicity and variations of seismic parameters as the *b* value and the energy rate occurred, testifying the presence of evolutive trends in the seismic catalogue. Earthquakes in this area are not particularly strong, but, due to their shallow depths and to the high urbanization of the area, they can cause significant concern and damages. Based on chronicles of historical eruptions, the maximum level of expected magnitude is around 4, large enough to cause significant damages to the ancient Roman towns of Pompeii and Herculaneum, and serious concern and problems also today. We have explored the possibility of intermediate-term earthquake prediction at Mt. Vesuvius using the CN algorithm (*Keilis-Borok and Rotwain*, 1990). The algorithm has been applied to the OVO station earthquake catalogue of Mt. Vesuvius seismicity (*De Natale et al*, 2002, 2004), available since 1972. The prediction CN algorithm identifies the Time of Increased Probability (TIP) for the occurrence of earthquakes with magnitude $M \geq M_0$, where M_0 is a numerical threshold that is chosen, for each studied region, according to its seismicity level.

The CN algorithm has been formulated for the California-Nevada region, considering $M_0 = 6.4$, while the Mt. Vesuvius zone is characterized by a low level of seismicity. Therefore the application of CN for the prediction of so small-magnitude events may require the time and space rescaling of the algorithm.

The rescaling of the precursor's zone accordingly to M_0 (*Keilis-Borok and Kossobokov*, 1990) cannot be applied to the Mt. Vesuvius because OVO catalogue covers a well-defined volume of about 6x6x8 km^3 (*De Natale et al.*, 2000) around the volcano and does not report the space coordinates of the events.

Keilis-Borok (1996) argues that the time scaling, depending on M_0, is not required by prediction algorithms CN and M8 (*Keilis-Borok and Kossobokov*, 1990), on the base of the following considerations. The earthquakes with smaller magnitudes occur more frequently, accordingly to the Gutenberg-Richter (G-R) relation, and the average time between the earthquakes of magnitude M is proportional to 10^{bM}. On the other hand the G-R law refers to a given region, the same for all magnitudes, while premonitory patterns are defined for an area with linear dimensions proportional to 10^{aMo}, where a is about (0.5 – 1) times the characteristic length of its sources (*Kanamori and Anderson*, 1975; *Båth*, 1981). Therefore the average time between the earthquakes in such an area (the precursor's zone at the intermediate-term medium-range stage) would be proportional to $10^{(b-a\nu)Mo}$, where ν is the fractal dimension of the cloud of the epicenters (*Kagan and Knopoff*, 1980; *Kagan*, 1991; *Kossobokov and Mazhkenov*, 1994). The existing estimations of the parameters b (≈ 1), a (0.5 – 1), and ν (1.2 – 2) for tectonic earthquakes do not contradict the hypothesis that the expression (b-$a\nu$) is close to 0, hence earthquakes with different magnitudes have about the same recurrence time in their own preparation area (the intermediate-term medium-range precursor's zone). On the contrary, if $(b-a\nu) \neq 0$ then a time scaling is necessary.

In the case of the Mt. Vesuvius zone, we don’t know a priori whether a time scaling is required, since a straightforward estimation of the coefficient (b-$a\nu$) is impossible. In fact, the OVO catalogue does not contain the hypocentral coordinates and this prevents the calculation of the fractal dimension of the space distribution of the epicenters. In the well defined volume occupied by the seismicity of the Mt. Vesuvius zone, the reocurrence time for the events with $M \geq M_0$ could be calculated directly from the catalogue, without a and ν estimation, if the length of the catalogue is adequate, but OVO catalogue covers a too short period of time. Therefore, we have to solve empirically the problem of time scaling, depending on M_0, directly by changing the time windows, over which the functions and TIPs in CN are estimated, and by comparison of the different prediction results.

2. CN algorithm

The intermediate-term earthquake prediction CN algorithm and its application to predict of strong earthquakes in different regions wordwide have been described in several papers (e.g. *Keilis-Borok et al.*, 1988; *De Becker et al.*, 1989; *Keilis-Borok and Rotwain*, 1989, *Keilis-Borok and Rotwain*, 1990, *Bhatia et al.*, 1990; *Keilis-Borok et al.*, 1990; *Arieh et al.*, 1992; *Gahalaut et al.*, 1992, *Panza et al.*, 1993; *Girardin and Rotwain*, 1994; *Costa et al.*, 1996, *Novikova et al.,* 1996; *Herak et al.*, 1999, *Peresan et al.*, 1999, *Peresan et al.*, 2004). Hence only a brief description of the algorithm is provided in this section.

The CN algorithm diagnoses the time of increased probability (TIP) of a strong earthquake in considered region. A strong earthquake is defined by the condition $M \geq M_0$, where M_0 is a numerical threshold. M_0 is chosen in each region in such a way, that the events with $M \geq M_0$ have an average return time of about 6-7 years. If this condition is satisfy we used also additional condition that value M_0 should be correspondend a local minimum in the histogram of the number of main shocks. The second condition provides the certain stabilities of the prediction results with respect to the choice of the threshold M_0.

The diagnosis is based on the following premonitory phenomena, characterised the seismic flow in the considered region: the level of the seismic activity, its variation in time, clustering of earthquakes in space and time, and their concentration in space.

Each of these premonitory phenomena is represented by a set of empirical functions, which are evaluated in a sliding time windows of length *s*. The list of these functions and their formal definitions are represented in Table 1. In the computation of the functions the aftershocks are not considered, but the number of aftershocks with $M \geq M_a$ is included as an one of the function, *Bmax*, measuring the earthquake clustering. The value of M_a should sutisfy the condition $M_a = \max\{(M_0 - 3), 0\}$.

The functions are normalized, so that their definition can be applied uniformly to regions with different size and level of seismicity. The normalization is achieved by the choice of the magnitude range $\underline{M} \leq M \leq \overline{M}$ for the events to be used in the computation of the functions. Here $\underline{M}$ is defined by condition that the avarage annual number of earthquakes with $M \geq \underline{M}$ in the considered region is equal to a constant $n(\underline{M})$, which is a common for all region; $\overline{M}$ is defined as $(M_0 - c)$, where $c = 0.1$ is also the common for all regions.

Consequently earthquake flow within the considered region at the moment *t* is represented by a vector formed by the values of the different functions listed in Table1. Accordingly to the pattern recognition method "Cora"(*Bongard*, 1967; *Gelfand et al*., 1976; *Keilis-Borok and Rotwain*, 1990) that was use in CN algorithm, such vector should be represented as binary vector. For that the considered period is divided into intervals denoted as *D*, *N* and *X*. Intervals *D* occupy two years before each strong event. After each strong event three years make up the *X* intervals. Intervals *X* can become intervals *D* if a next strong earthquake occures within the two years. The remaining time intervals are termed *N*. Functions are calculated for each moment with step one year during *D* and *N* intervals. The range of values of each function is discretized into three intervals, 'small', 'medium' and 'large' or into two intervals, 'small' and 'large'. The thresholds for the discretization of the functions are automatically determined in such a way that each interval of the function's values contains approximately the same number of moments from both D and N intervals. In other words, the discretization into three intervals is based on the quantile levels of 1/3 and 2/3; the discretization into two intervals based on the quantile level of 1/2.

The normalization and discretization of functions is made during the threshold-setting period (TSP).

The analysis of California-Nevada seismicity by the pattern recognition method permitted to define two sets of combinations of discretized functions (characteristic features). One set, *D*-features (*Keilis-Borok and Rotwain*, 1990, table 5), is typical for the *D* intervals, while another, *N*-features (*Keilis-Borok and Rotwain*, 1990, table 6), is typical for *N* intervals.

A TIP is announced by CN at the moment *t* for 1 year if two conditions are fulfilled:

1. $\Delta(t) \equiv n_D - n_N \geq \overline{\Delta}$, where n_D and n_N are the number of *D* and *N* features at the time *t*, respectively;
2. $\sigma(t) \equiv \Sigma_i(10^{M_i})/10^{M_o} < \overline{\sigma}$, here M_i is the magnitude of the i-th main shock, which occurred in the time interval of 3 years before moment *t*. The function $\Sigma(10^{M_i})$ is roughly proportional to the total area of the relevant fault rupture.

Subsequent TIPs can overlap and thus extend the alarm time beyond one year. A TIP is named as a false alarm if a strong earthquake does not occur during the TIP; if a strong earthquake does not preceded by TIP, we name it as a failure-to-predict.

Numercal thresholds, $\overline{\Delta}$, $\overline{\sigma}$ and parameters of definition of the functions listed in Table 1 are the parameters of the CN algorithm. The values of them were defined by the analysis of California-Nevada seismicity ($\overline{\Delta} = 5$, $\overline{\sigma} = 4.9$, values of other parameters are given in Table 2).

Following *Molchan* (1990), we will characterize the quality of the prediction results by the value $\varepsilon = (1 - \eta - \tau)$. Here $\eta = (1 - n/N)$, where *n* is the number of predicted earthquakes, and *N* is the total number of strong earthquakes; $\tau = t_\Sigma / T$, where t_Σ is the total duration of TIPs, and *T* is the total considered time. The result of the prediction is random if ($\eta + \tau$) = 1. An additional measure of the prediction quality is the statistics of false alarm, $\kappa = k/K$, where k is the number of false alarms, and K is the total number of alarms.

CN algorithm has been tested in 22 regions of the World with different dimensions and level of seismicity. Before CN application in each region we have to specify the following 'region-specific' conditions: (1) the boundary of the region covered by prediction; (2) the catalog to be used, and (3) the magnitude range M_0 of the earthquakes to be predicted. For each region we apply the same D and N characteristic features which were defined in California Nevada and given in *Keilis-Borok and Rotwain* (1990). For each region we repeat the procedure of discretization of functions as described above, since these features are given in terms of discrete values of the functions (i.e. "small", "medium" and "large"). All other parameters of CN algorithm are fixed. The results of this test show that TIPs cover about 30% of the total time and precede about 80% of the strong earthquakes. For the applications of CN in different regions of the World the statistics (1-η -τ) varies from 0.2 to 0.8, and κ varies from 0 to 0.67.

3. CN variant suitable for volcanic seismicity

We defined the region-specific condition for Mt. Vesuvius as follows:

1. *Boundaries of the region*. No formal boundaries are defined, because the earthquakes at Mt. Vesuvius are localized within a very narrow space volume.

2. *Catalog*. Two catalogs of vesuvian earthquakes are considered: the OVO catalog revised and described by *De Natale et al*. (2002, 2004), referred below as the "main" catalog, and the OVO catalog retrieved from the web site: www.ov.ingv.it/italiano/frm_ingv_ov.htm?../ufmonitoraggio/italiano/analisi/catalogo/ultimo.

3. *Magnitude range M_0*. As mentioned above the value of M_0 has to be defined accordingly

the condition that the events with M ≥ M_0 have average return time of about 6-7 years. Therefore the value of M_0 is depend from time scaling. So we can't define this value a formally a'priory. Note only, that a local minimum in the histogram of the number main shocks (Fig.3) correspond to M = 3.1 therefore we define the possible range for M_0 as 3.0 - 3.3.

The application of the CN algorithm to seismicity with a so small M_0 ($3.0 \leq M_0 \leq 3.3$) requires the following ajusting of the CN parameters.

- The condition for the identification of TIPs, $\sigma(t) \leq \underline{\sigma} = 4.9$ was introduced for tectonic earthquakes, to reduce the number of false alarms, and it is based on the energy released in the 3 years preceding the time *t*. For volcanic seismicity, where the strong earthquakes appear highly clustered in time, this condition does not seem to be appropriate. Therefore we take $\underline{\sigma} = \infty$.

- We introduce the time scaling for CN application. For that we make several prediction experiments changing the durations of the time windows used in CN algorithm to reduce them by a factor ϑ. In other words, each function, described above, is calculated during the time window of length s/ϑ, with respect to the standard value *s*, and a TIP is announced for $12/\vartheta$ months, instead of the standard 1 year. Several values of ϑ are tested, varying from 1 to 3.5 with step 0.5, and, for every value of ϑ, the CN algorithm is applied considering M_0 = 3.0, 3.1, 3.2, 3.3.

Thus, we have the following three adjusting parameters: M_0, $\underline{\sigma}$, and ϑ. As in other regions where CN was applied, all other parameters of the algorithm, including D and N features (see *Keilis-Borok and Rotwain*, 1990, table 5 and 6), remain fixed. The influence of choices of these three parameters on the prediction results will be considered in Section 5.

4. Data

The main OVO catalogue based on the records of the OVO station, installed in 1972 by the Osservatorio Vesuviano. The version of this catalog considered for the retrospective analysis by CN algorithm, covers the period from 23.02.1972 to 12.10.2002 and contains 9478 events. The last updated version of the catalogue available for tests of prediction in advance extends up to June 2004. The general properties of the main OVO catalog are given below; detailed information about this data set can be found in *De Natale et al.* (2002 and 2004).

The web site version of OVO catalogue covers the same period and contains 9203 events. The principal differences between these two catalogues for events with $M \geq 2.0$ are the following. Web site version contains 6 additional events and has a several discrepancies among aftershocks of earthquake 9.10.1999 with $M = 3.6$. Specifically, 5 out of 6 additional events have the magnitude $M \geq 3.0$: 29.09.1977, $M = 3.0$; 21.10.1977, $M = 3.1$; 19.11.1978, $M = 3.3$; 20.11.1978, $M = 3.3$ and 22.02.1979, $M = 3.0$. One additional earthquake, 7.31.1978, has $M = 2.8$.

The equipment of the OVO station is unchanged since its installation and the same magnitude type (M_d) is reported for all events. The number of earthquakes for the different ranges of magnitude versus time is given in Fig. 1. The magnitude-frequency distribution for the seismicity in Mt. Vesuvius zone is characterised by a large *b*-value (Fig.2), which is quite typical for volcanic seismicity (e.g. *De Natale et al.*, 2002; *Zollo et al.*, 2002). Nevertheless a time dependent estimation of the *b*-value evidences a well-defined pattern, with values of *b* progressively decreasing, from about 1.8, at the beginning of the considered period, to about 1 at present (*De Natale et al*., 2002; *Zollo et al.*, 2002; *De Natale et al*., 2004). The *b*-values determined in volcanic areas are generally higher than in tectonic ones (*Minakami,* 1974). *Scholz* (1968) explained the high values of *b* as related to high stress intensity, typical for volcanic swarms. Recent studies and laboratory experiments, however, indicate that *b*-values can significantly decrease in volcanic areas, during continuous fracturing, as a consequence of the fracture coalescence generating progressively larger faults (*Meredith et al.,* 1990; *Wyss et al.*, 1997). The most recent research, actually, tends to interpret the occurrence of an eruption as the time at which the fractures connecting the magma chamber and the surface are formed (*Kilburn and Voight,* 1998). In this framework, an eruption could be forecasted by increasing seismicity, with increasing magnitude and decreasing *b*-value.

A low level of seismicity characterises the zone of Mt. Vesuvius. The maximum magnitude of the earthquakes since 1972 is 3.6. A histogram of the number of main shocks with magnitude $M \geq 2.0$, and $\Delta M = 0.1$ given in Fig.3. The list of the main shocks with $M \geq 3.0$ is given in Table 3. The distribution in time of these strong main shocks (Fig.4) demonstrates the abnormal clustering of events in time. This problem was discussed by *De Natale and Zollo* (1986), *Godano et al.* (1997), *Zollo et al*. (2002).

5. The prediction results using the main catalogue.

A set of experiments has been performed, applying CN algorithm for the diagnosis of TIPs at Mt. Vesuvius during the period 1973 – 2002. The prediction of earthquakes, occurred in the past, is indicated as "retrospective prediction". The quality of retrospective prediction results versus ϑ is shown in Fig.5. One can see that $\vartheta = 2.5$ and $\vartheta = 3$ provide the best quality for all of the selected values of M_0, while the results are nearly random $((\eta + \tau) > 0.83)$ when the time scaling is absent $(\vartheta = 1)$.

The best quality results of CN retrospective application ($\vartheta = 3$ and 2.5, $M_0 = 3.0 - 3.3$) are shown in Fig.6 and summarized in Table 4. All strong earthquakes are predicted, with the exception of earthquake 5.11.1997, $M = 3.0$. The duration of TIPs varies from 31% to 33% of the total time for different M_0.

The number of false alarms is relatively large, about half of which are the continuation of alarms after strong earthquakes occurrence. Some persistent false alarms appear during the period from 1978 to 1986. Two reasons can be suggested as the explanation of that. The fist is the imperfection of the OVO catalogue during this period. The second one is the imperfection of the CN algorithm. A hight seismic activity, in any case, is not necessary associated with large magnitudes. Nevertheless the quality of these prediction results is similar to the quality of CN application in regions of tectonic seismic activity.

The lower level of magnitude for earthquake flow considered for calculation 7 out of 8 CN functions (with one exception *Bmax*) is $\underline{M}$ = 2.2 (n (2.2) = 3)); therefore $\underline{M}$ is fairly above the completeness threshold estimated for the OVO catalog.

6. Control experiments.

In this section we will discuss the influence of the variation of some adjusted CN parameters M_0 and $\overline{\sigma}$ on the prediction results as well as the stability of predictions with respect to the choice of the TSP and of the used catalog.

As we can see on Fig. 5 and 6 that the prediction results are quite stable with respect to variations of M_0 for ϑ = 2.5 and ϑ = 3.

These results depend on the variation of $\overline{\sigma}$, due to the second condition for TIP's declaration: $\sigma(t) \equiv \Sigma_i(10^{Mi})/10^{Mo} < \overline{\sigma}$. This condition denote that the released energy $\sigma(t)$, is lower than a quantity, $\overline{\sigma}$, corresponding to the energy of an earthquake with magnitude $M^* = M_0 + \Delta M$. The quality of prediction results, $(\eta+\tau)$, as a function of the values $(M^* - M_0)$ and M_0, is given in Table 5. For the value $\overline{\sigma}$ = 4.9 (i.e. $M^* - M_0$ = 0.69) the satisfactory quality of predictions appears when $M_0 \geq 3.1$. For M_0 = 3.0 the quality of the result is satisfactory only if $(M^* - M_0) \geq 0.9$ (i.e. $\overline{\sigma} \geq 7.9$). This fact comes out of the high clustering of earthquakes with $M \geq 3.0$.

To verify the validity of stability results, retrospective test named “Seismic History”, (*Gelfand et al.,* 1976) has been applied. This experiment shows how the variation of the seismic regime in the region affects to the prediction. For that the end of TSP is progressively shifted, step by step, so that TSP duration is reduced. The normalisation and discretization of the functions are repeated for each TSP. Other parameters of CN algorithm are keeped fixed. The quality of the prediction is verified for period after end of TSP, called as “test period”. In other words this experiment is a simulation of the prediction in advance when all CN parameters are defined and fixed a’priory to prediction.

The results of the experiment “Seismic History” for M_0 = 3.0 and ϑ=3 are given in Fig. 7 and summarized in Table 6. One can see that the (η + τ) value varies from 0.39 to 0.43 and slightly increases with decreasing TSP duration. When the end of TSP is shifted to 1989.10.24, only 3 strong earthquakes occurred during this period. Nevertheless 9 out of 10 the strong earthquakes are preceeded by TIP within the test period.

Two additional tests have been performed for the version of OVO catalog from the web site. First test deals with the variant of catalogue where five events with $M \geq 3$ (see section 4) has been deleted (1st version). Second test deals with the whole catalogue including five events with $M \geq 3$ (2nd version). The normalisation and discretization of the functions for both versions was repeated; all another CN parameters were fixed. Results of CN application is shown in Table 7. One shows that (η + τ) value slightly increases for M_0 from 3.1 to 3.3 in both tests, and becames significant greater for M_0 = 3.0 in the second test. Results of CN application for M_0 = 3.2, and M_0 = 3.3 shown in Fig. 8.

The parameters for CN application to the prediction of earthquakes at Mt. Vesuvius have been defined considering the catalog available up to October 21 2002 (*Rotwain et al.*, 2003). The test in advance predictions has been carried out since October 22 2002. The results obtained for different M_0 can be summarised as follows: during the period from 21.10. 2002 to 21.6.2004 no earthquakes with $M \geq 3.0$ occurred and no TIP have been declared by CN algorithm. Consequently the value of τ decreased, while the statistics of η and κ remain unchanged.

7. **Conclusions and discussion**

The experiments with seismicity of Mt. Vesuvius described above show that the CN algorithm is appropriate for the prediction of strong earthquakes in volcanic areas.

The quality of the prediction for earthquakes with $M \geq 3.0$ at Mt. Vesuvius zone is similar to the quality of the prediction of strong earthquakes in different tectonic regions worldwide.

The results of the experiment "Seismic History" allow us to assume a good quality for the forward prediction, and CN could be applied for the monitoring of the volcano seismicity with the continuously updated OVO catalogue.

The successful application of the CN algorithm for the prediction of earthquakes at the Mt. Vesuvius zone shows that the difference in the preparation of strong earthquakes in volcanic areas is not essential from the point of view of prediction results. Moreover the good quality of predictions for such small earthquakes, obtained by simply decreasing the time windows of the algorithm accordingly to the decrease of M_0, is an evidence of self-similarity in the process of earthquakes preparation.

The introduction of the time scaling in the CN algorithm for the prediction of earthquakes with M_0 = 3.0 - 3.3 shows that the best prediction's results for Mt. Vesuvius zone is obtained when the duration of the time windows is reduced by a factor 2.5 - 3. Possibly the same rescaling approach will be useful for the prediction of tectonic earthquakes in regions with the similar values of M_0. Tests demonstrated that the web site catalog could be used for the routine monitoring.

Successful cases of eruptions predicted on the base of the *b* value changes, the stress release, the power law exponent, and the fractal dimension variations are reported (*Malone et al.,* 1983;

Gresta and Patane, 1983; *Vinciguerra,* 1999, 2002; *Hill et al.* 2002). The question arises whether the forecast of the larger earthquakes is in some way related to the possibility to forecast eruptions, i.e., whether the occurrence of the larger earthquakes can be considered as an eruption precursor. Although the historical evidence points out the absence of very large magnitude earthquakes in this area (with maximum magnitudes around 4), it is probable that the largest seismic rate and earthquake magnitude occurred before the largest eruptions *(Marturano and Rinaldis*, 1996). Moreover, *Esposito et al*. (2000) pointed out generally low *b*-values (around 1.0) before the major historical eruptions. In this perspective, it is likely that periods of more intense seismicity with larger magnitude are also periods with higher probability of eruption. If this is true, the forecast of larger earthquakes is also an important tool to help in the forecast of eruptive events.

Nevetheless one may question whether a complex prediction algorithm like CN is necessary for the prediction of volcanic earthquakes, since it is known that for volcanic earthquake-swarms, , like those associated to the Vesuvius strong events, the seismic activity starts with an increasing number of earthquakes and then decreases after the largest one. Fig. 9 displays the number of earthquakes with $M \geq 2.0$ vs. time. At least four earthquakes with $M \geq 3.0$ are not preceded by a large number of small events; the same happens for two out of four earthquakes with $M \geq 3.3$, including the strongest earthquake with $M = 3.6$. Therefore the predictive capability, based on the increased number of small events only, seems quite unsatisfactory for Vesuvian earthquakes. Moreover, the prediction of strong earthquakes based only on the function of the number of earthquake (N(t| $\underline{M}$, s)) would require to adjust several parameters (e.g. whether to use the whole catalog or catalog of main shocks only; the threshold for declaration of alarm; be formulated based on retrospective analysis sould be designed and tested in different regions and by in advance.

Acknowledgments

We acknowledge the financial support from the Abdus Salam International Centre for Theoretical Physics in Trieste, Italy, from GNV (Gruppo Nazionale Vulcanologia), Italy, and from MNTC project n°1538, and SfP NATO Project 972266. Part of this research has been developed in the framework of the INGV Project - Eruptive Scenarios from Physical Modeling and Experimental Volcanology.

References

Arieh, E., I. Rotwain, J. Steinberg, I. Vorobieva, F. Abramovich. (1992), Diagnosis of Time of Increased Probability of strong earthquakes in the Jordan-Dead sea rift zone. Tectonophysics, vol.202, 351-359.

Båth, M, (1981), Earthquake magnitude-recent research and current trends. Earth-Science Review, 17, 315-398

Bhatia, S., Vorobieva, I., Gaur, V. K., Levshina T. A., Subedi L., Chalam, S. (1990), Diagnosis of times of increased probability of strong earthquakes in the Himalayan seismic belt by CN algorithm. Analysis of geophysical fields. Moscow, Nauka, English translation in computational Seismology and Geodynamic, vol. 23, 25-30.

Bongard, M.M., (1967), The Problem of Recognition. Moscow, Nauka, 320p. (in Russian).

Costa, G., I.Orozova-Stanishkova, G.F.Panza, I.Rotwain. (1996), Seismotectonic Models and CN Algorithm: The case of Italy. Pure and Appl. Geophys., 147 (1), 119-130.

De Becker, M., O. Dmitrieva, V. I. Keilis-Borok and I. M. Rotwain. (1989), Premonitory seismicity pattern in a platform region. (Ardennes, Rhenish and Braband massifs, lower Rhine graben) Phys. Earth Plane. Inter., 57, 260-265.

De Natale, G., *and A. Zollo.* (1986), Statistical analysis and clustering features of the Phlegrean fields earthquake sequence (May 1983 – May 1984), Bull. Seism. Soc. Am., 76, 801-814.

De Natale G., Capuano P., Troise C. and Zollo A. (1998), Seismicity at Somma-Vesuvius and its implications for the 3D tomography of the volcano. J. Volcanol. Geotherm. Res., Special Issue Vesuvius. Spera F. J., De Vivo B., Ayuso R.A., Belkin H.E. (Eds), 82 (1-4): 175-197.

De Natale, G., *S. Petrazzuoli, C. Troise, F. Pingue, and P. Capuano*. (2000), Internal stress field at Mount Vesuvius: a model for background seismicity at a central volcano. Journal of Geophys.

Research, vol. 105, No. B7, 16207-16214.

De Natale, G., Kuznetsov I., Kronrod, T., Peresan, A., Sarao, A., Troise, C., Panza, G. (2002), Three decades of seismic activity at Mt. Vesuvius: 1972-1999. Preprint of the Abdus Salam International Centre for Theoretical Physics, IC/2002/45, 39.

De Natale, G., Kuznetsov I., Kronrod, T., Peresan, A., Sarao, A., Troise, C., Panza, G. (2004), Three decades of seismic activity at Mt. Vesuvius: 1972-1999, Pure and Appl. Geophysics, 161, 123-144.

Esposito, E., Mastrolorenzo, G. and Porfido, S. (2000), Seismicity at Vesuvius, a comparison between historical eruptive periods and present time. Abstract. EGS 2000. Nizza, France.

Gahalaut, V.K., I.V. Kuznetsov, I.M.Rotwain, I.M. Gabrielov, V.I. Keilis-Borok. (1992), Application of pattern recognition algorithm in the seismic belts of Indian convergent plate margin - CN algorithm, *Proc. Indian Acad. Sci.*, vol. 101.

Gelfand, I. M., Guberman, Sh. A., Keilis-Borok, V. I. Knopoff, L., Press, F., Ranzman, E. Ya., Rotwain, I. M., Sadovsky, A. M. (1976), Pattern recognition applied to earthquake epicentres in California. Phys. Earth Planet. Inter., 11, 227-283.

Girardin, N., and I. Rotwain (1994) Diagnosis of the time of increased probability of earthquakes of Magnitude 5.5 or greater in the Lesser Antillean arc. Phys. Earth Planet. Inter., vol. 83, 57-65.

Godano, C., M. L. Alonzo, and G. Virardo. (1997), Multyfractal approach to time clustering of earthquakes. Application to Mt. Vesuvio seismicity, PAGEOPH, 149, 375-390.

Gresta, S. and G.Patane. (1983), Change in *b* value before the Etnean eruption of March-August 1983. Pure and Appl. Geophysics, 121, 903-912.

Herak, D., Herak, M., Panza, G.F., and Costa, G. (1999), Application of the CN Intermediate-term Earthquake Prediction Algorithm to the Area of the Southern External Dinarides. Pure and Appl. Geophysics, 156, 689-699.

Hill, D. P., Pollitz F. and Newhall Ch. (2002), Earthquake-Volcano Interactions. Physics Today, vol. 53, No 11, November, 41-54.

Kagan, Y. Y. and L. Knopoff. (1980), Spatial distribution of earthquakes: The two-point correlation function. J.Roy. Astr. Soc., 62, 303-320.

Kagan, Y. Y. (1991), Fractal dimension of brittle fracture. J. Nonlinear Sci., 1, 1-16.

Kanamori, H., and D.L. Anderson. (1975), Theoretical basis of some empirical relations in seismology. Bulletin of the Seismological Seismicity of America, Vol.65 (5), 1073-1095

Keilis-Borok, V *.I.* (1996*),* Intermediate-term earthquake prediction. Proc. Natl. Acad. Sci. USA, vol. 93, 3748-3755.

Keilis-Borok, V *.I., L. Knopoff, I. M. Rotwain & C. Allen.* (1988), Intermediate-term prediction of occurrence times of strong earthquakes, Nature, 335, 6192, 690-694.

Keilis-Borok, V. I., and V. G. Kossobokov. (1990), Premonitory activation of earthquake flow: algorithm M8. Phys. Earth Planet. Inter., 61, 1-2: 73-83.

Keilis-Borok, V. I., and I. M. Rotwain. (1989), Diagnosis of increased probability of strong earthquakes in Northern Appalachians. Comput. Seismol., 22, 9-18.

Keilis-Borok, V.I., L. Knopoff, V. Kossobokov, and I. Rotwain. (1990a), Intermediate-term prediction in advance of the Loma Prieta earthquake. Geophysical research letter, v.17, No.9.

Keilis-Borok, V. I., I. V. Kuznetzov, G. F. Panza, I. M. Rotwain, and G. Costa. (1990b), On intermediate-term earthquake prediction in Central Italy. PAGEOPH, 1990, 134, 1, 79-92.

Keilis-Borok, V. I., and I. M. Rotwain (1990), Diagnosis of Time of Increased Probability of strong earthquakes in different region on the world: CN algorithm, Phys. Earth Planet. Inter., 61, 57-73.

Kilburn C.R.J. and Voight B. (1998), Slow rock fracture as eruption precursor at Soufriere Hills volcano, Montserrat. Geophys Res Letters, 19: 3665-3668.

Kossobokov, V. G., and S .A.. Mazhkenov. (1994), On similarity in the spatial distribution of seismicity. Computational Seismology and Geodynamics. Vol. 1, 6-15.

Malone, S. D., C. Boyko, C. S. Weaver. (1983), Seismic precursors to the Mount St. Helens eruption in 1981 and 1982. Science, 221, September, 1376-1378.

Marturano, A. and Rinaldis, V. (1996), Seismic history and consistent seismicity; evidence from southern Italy. Natural Hazards, 14, 11-21.

Meredith P.G., Main I.G. and Jones C. (1990), Temporal variations in seismicity during quasi-static and dynamic rock failure, Tectonophysics, 175, 249-268.

Minakami, T. (1974), Seismology of volcanoes in Japan. In: Civetta et al. (Eds.) Physical Volcanology Developments in Solid Earth Geophysics vol 6. Elsevier Amsterdam pp 1-27.

Molchan G. M. (1990), Strategies in strong earthquake prediction. Phys. Earth Planet. Inter., 61, 84-98.

Novikova, O.V., Vorobieva, I.A., Enescu, D., Radulian, M., Kuznetsov, I., Panza, G.F. (1996), Prediction of the strong earthquakes in Vrancea, Romania. Pure and Appl. Geophys, 147(1), 99-118.

Panza, G. F., I. Orozova-Stanishkova, G. Costa, I. Rotwain, F. Vaccari. (1993), Intermediate-term earthquake prediction and seismic zoning in Northern Italy. Second Workshop on Non-Linear Dynamics and Earthquake prediction. International Centre for Theoretical Physics, Trieste, Italy, 1993.

Peresan A., Costa G. and Panza G.F. (1999), Seismotectonic model and CN earthquake prediction in Italy. Pure and Appl. Geophys. 154, 281-306.

Peresan A., Kossobokov V., Romashkova L., and Panza G.F. (2004), Intermediate-term middle-range earthquake predictions in Italy: a review. Earth Science Reviews. In press.

Rotwain I., De Natale G., Kuznetsov I., Peresan A., and Panza G.F. (2003), Diagnosis of time of increased probability of volcanic earthquakes at Mt.Vesuvius zone. Preprint of the Abdus Salam

International Centre for Theoretical Physics, IC/2003/21, 19.

Scholz, C. H. (1968), Microfractures, aftershocks and seismicity, Bull. Seismol. Soc. Am., 58, 1117-1130.

Vilardo G., De Natale G., Milano G. and Coppa U. (1996), The seismicity of Mt. Vesuvius. Tectonophysics, 261, 127-138.

Vinciguerra, S. (1999), Scaling exponents as a tool in detecting stress corrosion crack growth leading to the September-October 1989 flank eruption at Mt. Etna volcano. Geophys. Res. Lett., 26, 3685-3688.

Vinciguerra, S. (2002), Damage mechanics preceding the September – October 1989 flank eruption at Mt. Etna volcano inferred by seismic scaling exponents. J. Volcanol. Geotherm. Res. 113, 391-397

Wyss, M., K. Shimazaki, S. Wiemer. (1997), Mapping active magma chambers by *b*-value beneath the off –Ito volcano. Japan J. Res., 102, 20413-20422.

Zhurkov S.N., Kuksenko V.S., Petrov V.A., Saveljev V.I., Sultanov U.S. (1978), Concentration criterion of volume-type fracture in solids. Physical processes in earthquake sources. M., Nauka, 101-106 (in russian).

Zollo, A., W. Marzocchi, P. Capuano, A. Lomax and G. Iannaccone. (2002), Space and time behavior of seismic activity at Mt. Vesuvius volcano, Southern Italy.Bull. Seismol. Soc. Am., 92 (2), 625-640.

Figure captions

Fig.1. Histogram of the number of earthquakes as functions of time (time grouping 1 year) for different magnitude ranges.

Fig.2. Discrete frequency-magnitude distribution for different time periods (magnitude grouping 0.2). Each point on the graph corresponds to the number of earthquakes for magnitude interval shown on horizontal axis. Different symbols correspond to different periods.

Fig.3. Histogram of the number of main shocks for different magnitudes (magnitude grouping 0.1).

Fig. 4. Distribution of strong earthquakes in time, $M_d \geq 3.0$, for period 1972 – 2002.10. The vertical lines show the time of earthquake occurrence; its length shows the value of magnitude.

Fig.5. Dependence the quality of results on the time scaling factor ϑ for different M_0. Each point on the graph corresponds to the value of $(\eta + \tau)$ for some value of ϑ. Different symbols correspond to different M_0.

Fig.6. TIPs and strong earthquakes for $\vartheta = 3$ and 2.5 for different M_0: $M_0 = 3.0$ ($\vartheta = 3.0$); $M_0 = 3.1$ ($\vartheta = 2.5$); $M_0 = 3.2$ ($\vartheta = 2.5$); $M_0 = 3.3$ ($\vartheta = 3.0$). The TSP goes from 1972.2.23 to 2000.1.1. The vertical lines show the time of earthquake occurrence of earthquakes with $M \geq M_0$; its length shows the value of magnitude. The solid lines identify the earthquakes proceeded by TIP, the dashed lines identify the failure to predict. TIPs are marked by rectangles: black rectangle is a TIP preceded a strong earthquake, dashed rectangle is a false alarm.

Fig.7. TIPs and strong earthquakes in the "Seismic History" experiment for different endpoints of TSP. Symbols as in Fig. 6.

Fig.8. TIPs and strong earthquakes in test used the OVO web site catalogue for two values of M_0: $M_0 = 3.2$ (correspond to Table 7, #9)and $M_0 = 3.3$ (correspond to Table 7, #12). Symbols as in Fig.6.

Fig. 9. Number of earthquakes and strong shocks ($M \geq 3.0$) for the period from 1972 to 2004.6 accordingly main OVO catalog. Each point represents the value of function $N(t/\underline{M}, s)$ were $\underline{M} = 2.0$, $s = 4$ months. Vertical lines indicate the time of earthquake occurrence; its length shows the value of magnitude.

Table 1. List of CN functionals

#	Function	Definition
1	$N(t\vert \underline{M}, s)$	The number of main shocks with $M \geq \underline{M}$
2	$K(t\vert \underline{M}, s) =$ $N(t\vert \underline{M}, s) - N(t-s\vert \underline{M}, s)$	The difference between the number of main shocks at two successive time-intervals $(t\text{-}s, t)$ and $(t\text{-}2s, t\text{-}s)$
3	$G(t\vert \underline{M}_1, \underline{M}_2)=1 -$ $- N(t\vert\underline{M}_2, s)/N(t\vert\underline{M}_1, s)$	The ratio of the number of main shocks in two magnitude ranges $(\underline{M}_1, \underline{M}_2)$ and $M \geq \underline{M}_1$
4	$\Sigma(t\vert\underline{M}, \overline{M}, s, \alpha, \beta) =$ $\sum 10^{\beta(M_i - \alpha)}$	The number of main shocks weighted according to M_i. Summation is made on main shocks with $\overline{M} \geq M_i \geq \underline{M}$.
5	$Smax(t\vert\underline{M}, \overline{M}, s, u, \alpha, \beta) =$ $\max[\Sigma(t\vert\underline{M}, \overline{M}, s, \alpha, \beta)/$ $(N(t\vert \underline{M}, s) - N(t\vert \overline{M}, s))]$	Here $\beta = 1$, so that the expression in square brackets is roughly proportional to the average area of rupture in the source. The maximum value is taken within time-interval $(t\text{-}u, t)$
6	$Zmax(t\vert\underline{M}, \overline{M}, s, u, \alpha, \beta) =$ $\max[\Sigma(t\vert\underline{M}, \overline{M}, s, \alpha, \beta)/$ $[N(t\vert \underline{M}, s) - N(t\vert \overline{M}, s)]$	Here $\beta = 0.5$, so that the expression in square brackets is roughly proportional to the average linear dimension of the rupture in the source (*Zhurkov et al.*, 1978). The maximum value is taken within time-interval $(t\text{-}u, t)$
7	$q(t\vert \underline{M}, s, u) = \sum$POS $[N_{av}(\underline{M})\, s - N(t\vert \underline{M}, s)]$	The 'deficiency' of activity. Here "POS" indicates that the summa is taken only over positive value. Summation is made on main shocks with $M_i \geq \underline{M}$ within time-intervals $(t\text{-}s\text{-}u, t\text{-}s)$. N_{av} is the annual average number of main shocks.
8	$Bmax(t\vert\underline{M}, s, M_a, e) =$ $\max b_i(M_a, e)$	Here $b_i(M_a, e)$ is the number of aftershocks with $M \geq M_a$ within the period e after the main shock; The maximum value of b_i is taken for the main shocks with $M \geq \underline{M}$ from the time interval $(t\text{-}s, t)$

Table 2. Parameters of the definition of CN functions

#	Functions used	n(M)	s, years	Other parameters
1	$N2=N(t\vert \underline{M}, s)$	0.36	3	
2	$N3 = N(t\vert \underline{M}, s)$	1.4	3	
3	$K=K(t\vert \underline{M}, s)$	1.4	2	
4	$G=G(t\vert \underline{M_1}, \underline{M_2})$	3; 1.4	3	
5	$\Sigma=\Sigma(t\vert \underline{M}, \overline{M}, s, \alpha, \beta)$	3	3	$\overline{M} = M_0 - 0.1; \alpha=4.5; \beta = 1$
6	$Smax=Smax(t\vert \underline{M}, \overline{M}, s, u, \alpha, \beta)$	3	1	$\overline{M} = M_0 - 0.1; \alpha = 4.5; \beta = 1$
7	$Zmax=Zmax(t\vert \underline{M}, \overline{M}, s, u, \alpha, \beta)$	3	1	$\overline{M} = M_0 - 0.1; \alpha = 4.5; \beta = 0.5$
8	$q=q(t\vert \underline{M}, s, u)$	1.4	6	u = 3 yrs
9	$Bmax = Bmax(t\vert \underline{M}, s, M_a, e)$	-	-	$M_a = \max\{M_0 - 3{,}0\}$; e = 48 h

Table 3. List of main shocks with $M_d \geq 3.0$, for the period 1972. 2. 23 – 2002. 10. 12

#	Date	Time	Magnitude
1	29.01.1989	20:00	3.0
2	19.03.1989	19:22	3.3
3	21.10.1989	4:04	3.0
4	4.03.1990	23:39	3.0
5	8.07.1990	3:49	3.1
6	10.09.1990	23:58	3.3
7	2.08.1995	4:07	3.2
8	16.09.1995	11:03	3.2
9	25.04.1996	22:55	3.3
10	5.11.1997	11:28	3.0
11	9.10.1999	5:41	3.6
12	22. 01.2000	3:34	3.0
13	27.09.2000	7:01	3.0

Table 4. The results of the best quality prediction of strong earthquakes with $M \geq M_0$.

M_0	ϑ	n/N	η	τ	k/K	κ	$\eta+\tau$
3.0	3	12/13	0.08	0.31	7/19	0.37	0.39
3.1	2.5	7/7	0.0	0.31	7/14	0.50	0.31
3.2	2.5	6/6	0.0	0.32	7/13	0.53	0.32
3.3	3	4/4	0.0	0.33	7/11	0.64	0.33

Notes: n is the number of predicted earthquakes with $M \geq M_0$; N is the total number of main shocks with $M \geq M_0$; $\eta = n/N$ is the statistic of failure to predict; $\tau = \tau_\Sigma/T$ is the statistic of alarm time; k is the number of false alarms; K is the total number of alarms; $\kappa = k/K$ is the statistic of false alarm.

Table 5. Dependence of the prediction results quality ($\eta+\tau$) on the variation of the quantity (M^* - M_0) = 10^{σ}

M_0	M^* - M_0				
	0.69	0.8	0.9	1.0	∞
3.0	0.73	0.77	0.32	0.4	0.39
3.1	0.58	0.45	0.37	0.31	0.31
3.2	0.35	0.43	0.32	0.32	0.32
3.3	0.51	0.33	0.33	0.33	0.33

Notes: The values of ϑ for each $\boldsymbol{M_0}$ correspond to the result with the best quality: $\vartheta = 3$ for $\boldsymbol{M_0} = 3.0$ and $\boldsymbol{M_0} = 3.3$; $\vartheta = 2.5$ for $\boldsymbol{M_0} = 3.1$ and $\boldsymbol{M_0} = 3.2$

Table 6. Results of "Seismic History" experiment for M_0 = 3.0, ϑ = 3.

End of TSP	n/N	η	τ	k/K	κ	$\eta+\tau$	n_f/N_f
2000.1.1	12/13	0.08	0.31	7/19	0.37	0.39	2/2
1998.2.22	12/13	0.08	0.31	9/21	0.43	0.39	3/3
1996.6.24	11/13	0.15	0.24	6/17	0.35	0.4	3/4
1995.10.24	11/13	0.15	0.26	5/16	0.31	0.41	3/5
1990.10.24	11/13	0.15	0.27	6/17	0.35	0.43	5/7
1989.10.24	12/13	0.08	0.35	7/19	0.37	0.43	9/10

Notes: n is the number of predicted earthquakes with $M \geq 3$; N is the total number of main shocks with $M \geq 3$; $\eta = n/N$ is the statistic of failure to predict; $\tau = \tau_\Sigma/T$ is the statistic of alarm time; k is the number of false alarms; K is the total number of alarms; $\kappa = k/K$ is the statistic of false alarm; n_f is the number of predicted earthquakes which occurred during the test period; N_f is the total number of main shocks which occurred during the test period.

Table 7. The results of the prediction of strong earthquakes with $M \geq M_0$ for three versions of the OVO catalogue.

#	M_0	Versions of the catalogue	ϑ	n/N	η	τ	k/K	κ	$\eta+\tau$
1	3.0	main	3.0	12/13	0.08	0.31	7/19	0.37	0.39
2		1		11/13	0.16	0.28	7/18	0.4	0.44
3		2		13/17	0.23	0.39	11/24	0.4	0.62
4	3.1	main	2.5	7/7	0	0.31	7/14	0.5	0.31
5		1		7/7	0	0.31	6/13	0.46	0.31
6		2		8/9	0.11	0.3	6/14	0.43	0.41
7	3.2	main	2.5	6/6	0	0.32	7/13	0.54	0.32
8		1		6/6	0	0.32	6/12	0.5	0.32
9		2		7/7	0	0.33	7/14	0.5	0.33
10	3.3	main	3.0	4/4	0	0.33	7/11	0.64	0.33
11		1		4/4	0	0.31	7/11	0.64	0.31
12		2		5/5	0	0.34	6/11	0.54	0.34

Note: Main – main version;
1 – web site version, 5 earthquakes occurred during the period 1977 – 1979 were removed;
2 – web site version, including 5 strong events during the period 1977 - 1979.
All symbols are the same as in Table 4.

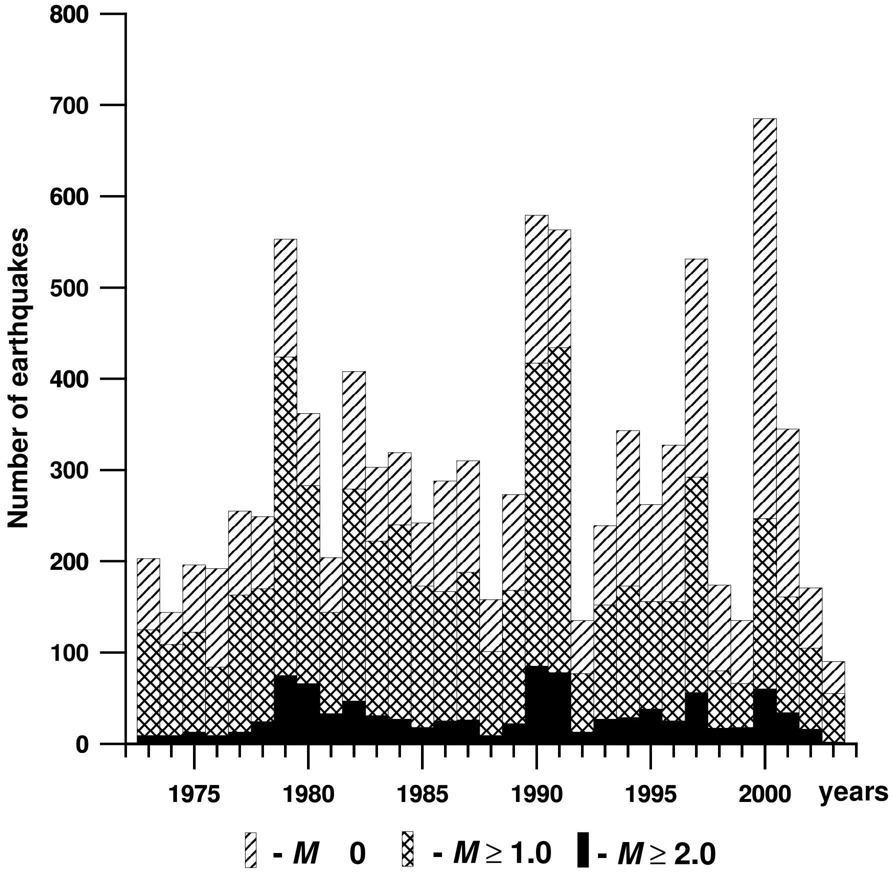

800
700
600
500
400
300
200
100
0
Number of earthquakes
1975
1980
1985
1990
1995
2000
years
- M 0
- M ≥ 1.0
- M ≥ 2.0

Fig.1

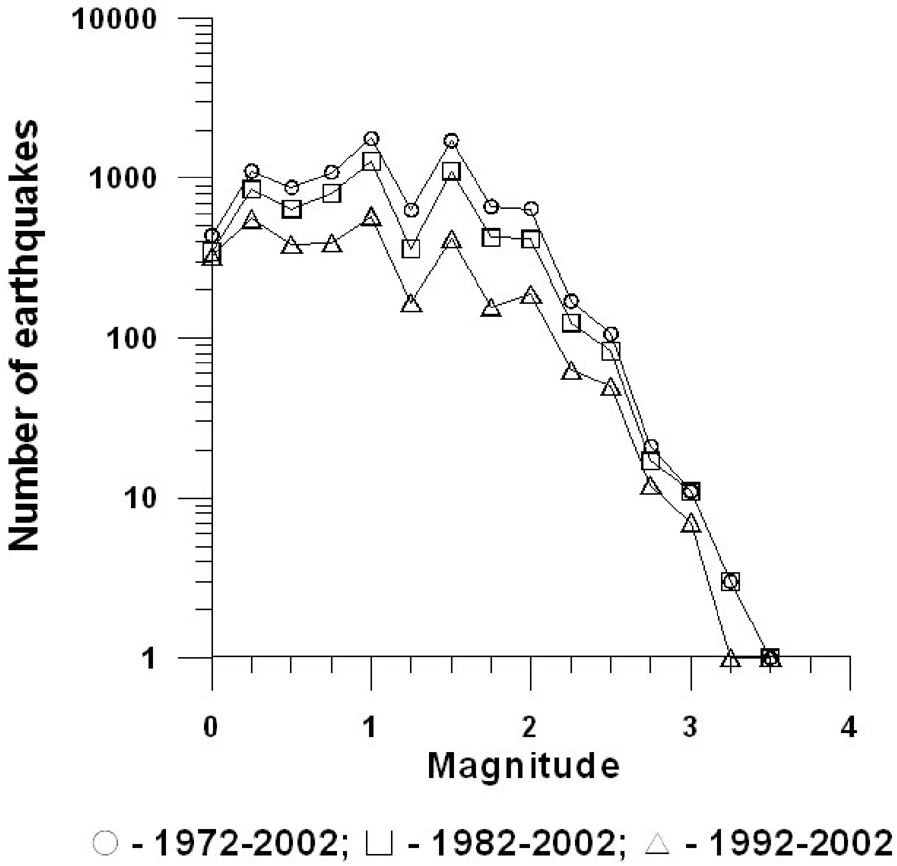
10000
1000
100
10
1
Number of earthquakes
0
1
2
3
4
Magnitude
○ - 1972-2002; □ - 1982-2002; △ - 1992-2002

Fig.2

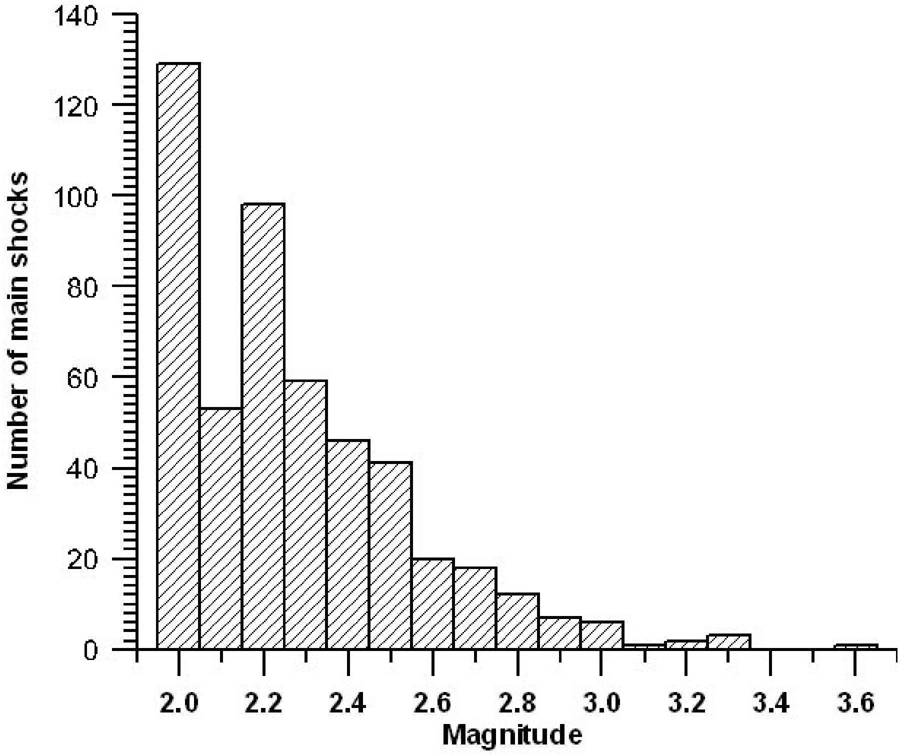

Number of main shocks
140
120
100
80
60
40
20
0
2.0
2.2
2.4
2.6
2.8
3.0
3.2
3.4
3.6
Magnitude

Fig.3

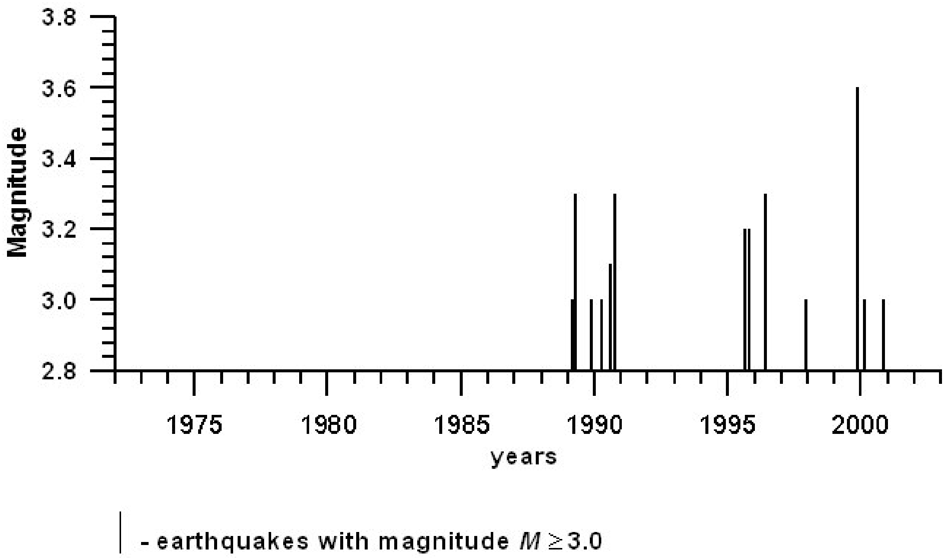

Magnitude
3.8
3.6
3.4
3.2
3.0
2.8
1975
1980
1985
1990
1995
2000
years
- earthquakes with magnitude $M \geq 3.0$

Fig.4

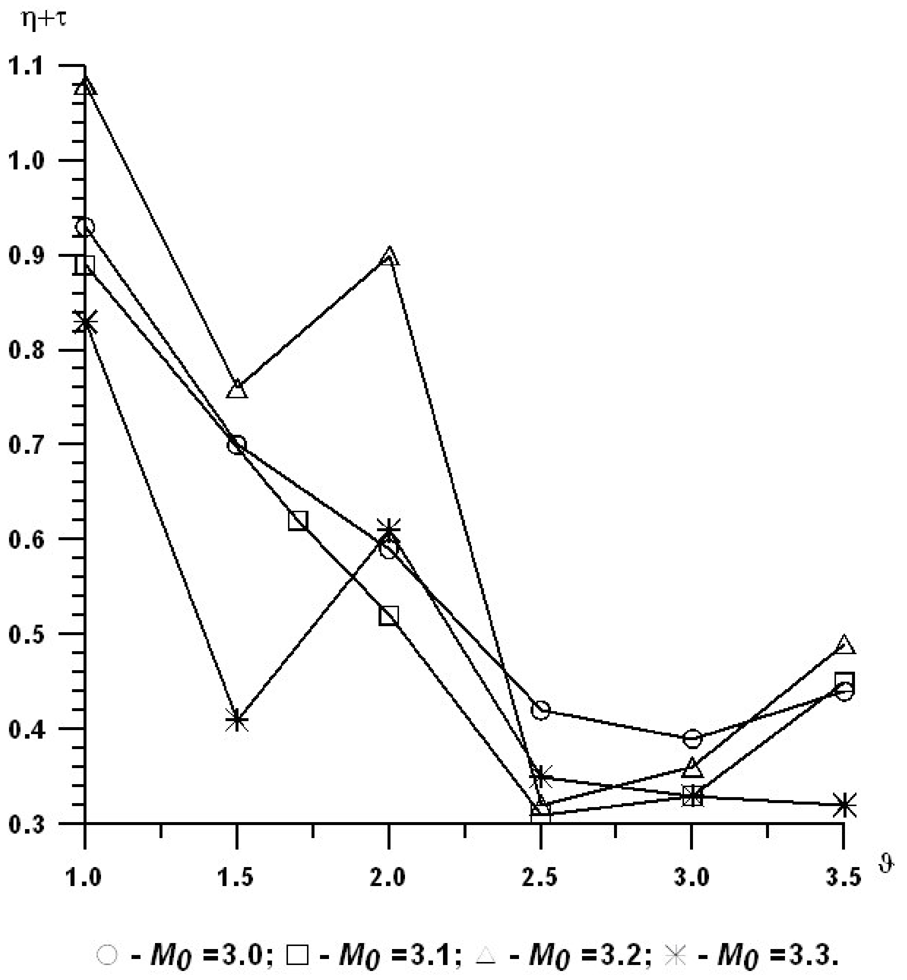

Fig.5

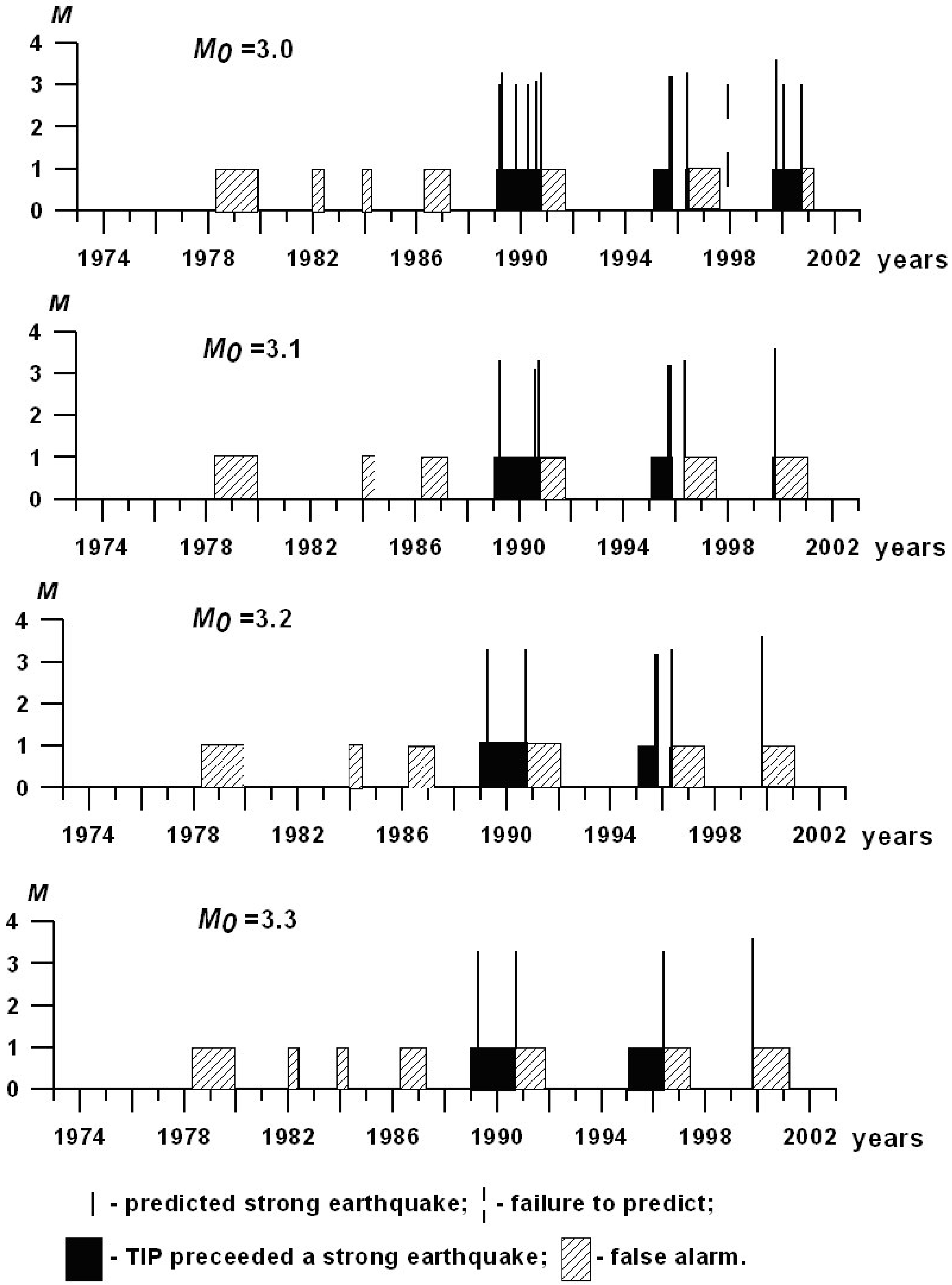
M
4
3
2
1
0
M_0 =3.0
1974
1978
1982
1986
1990
1994
1998
2002
years
M
M_0 =3.1
years
M
M_0 =3.2
years
M
M_0 =3.3
years
- predicted strong earthquake;
- failure to predict;
- TIP preceeded a strong earthquake;
- false alarm.

Fig.6

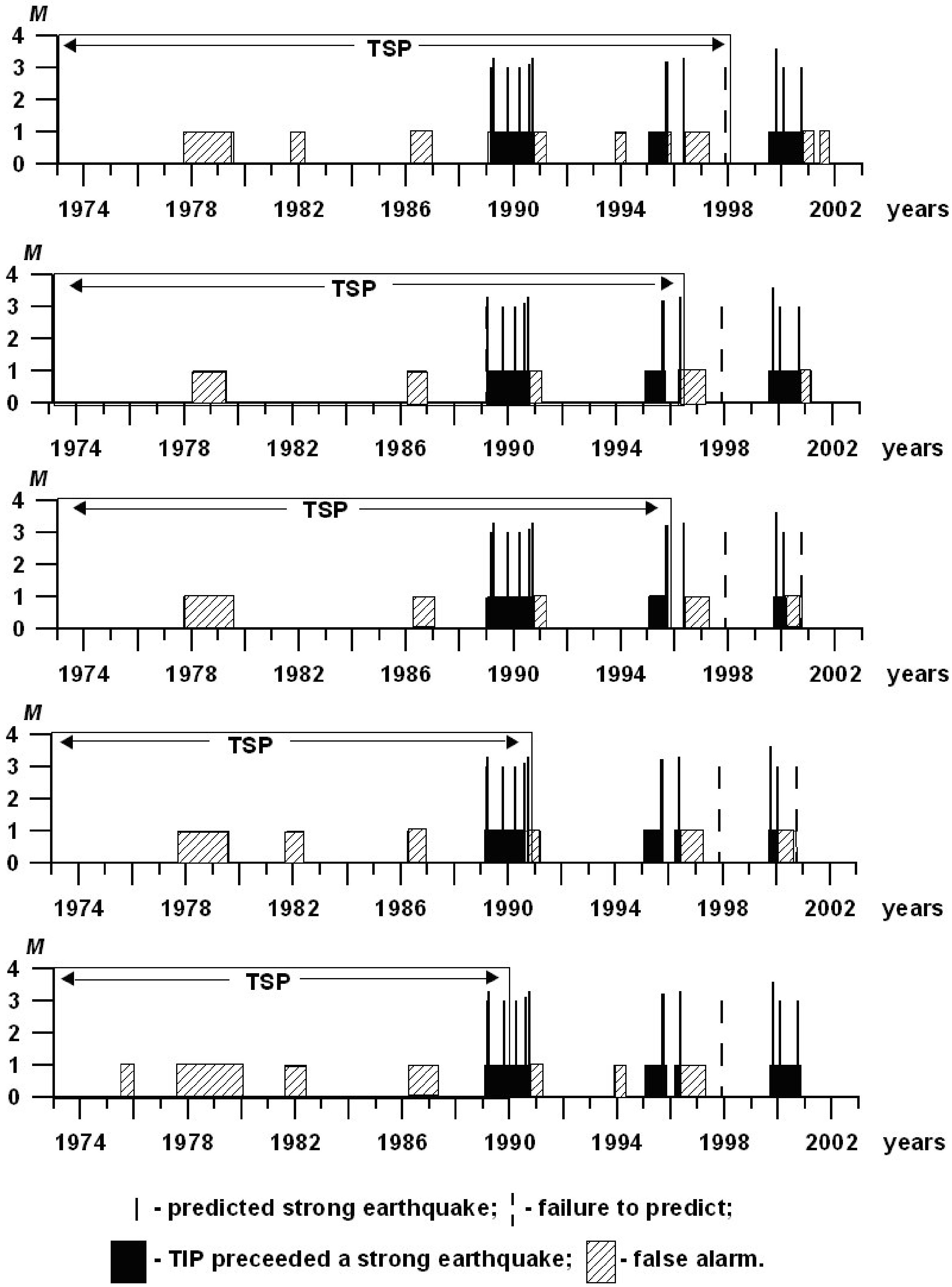
M
TSP
1974
1978
1982
1986
1990
1994
1998
2002
years
- predicted strong earthquake;
- failure to predict;
- TIP preceeded a strong earthquake;
- false alarm.

Fig.7

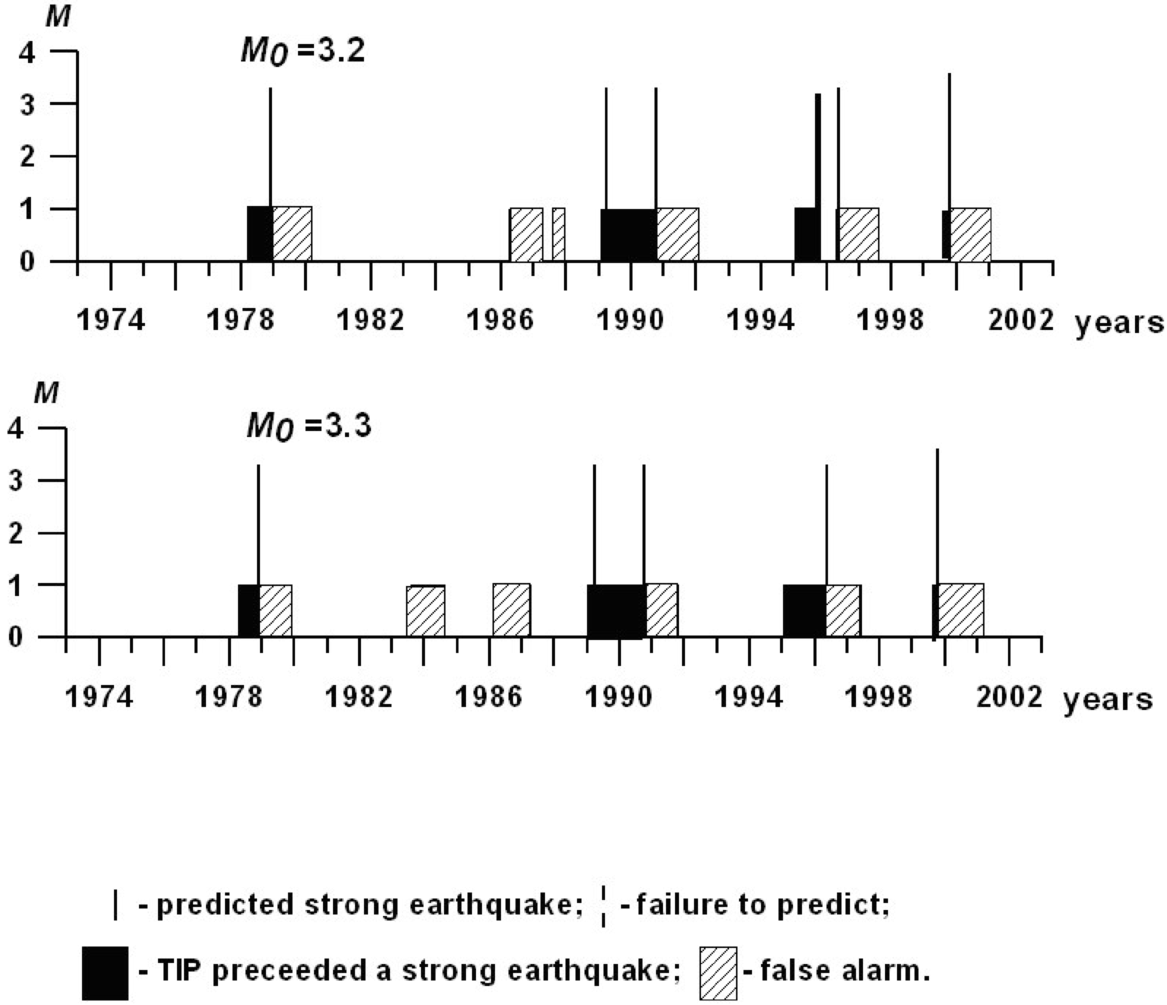
M
M_0 =3.2
4
3
2
1
0
1974
1978
1982
1986
1990
1994
1998
2002
years
M
M_0 =3.3
4
3
2
1
0
1974
1978
1982
1986
1990
1994
1998
2002
years
- predicted strong earthquake;
- failure to predict;
- TIP preceeded a strong earthquake;
- false alarm.

Fig.8

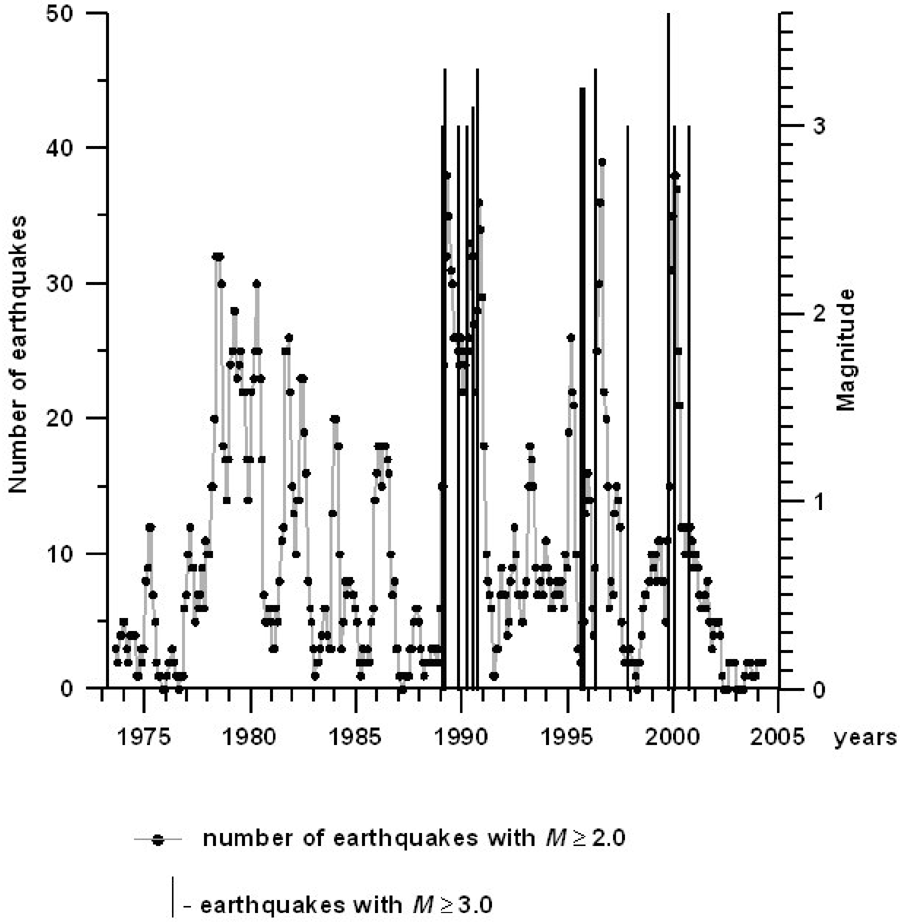
Number of earthquakes
Magnitude
years
50
40
30
20
10
0
3
2
1
0
1975
1980
1985
1990
1995
2000
2005
number of earthquakes with $M \geq 2.0$
- earthquakes with $M \geq 3.0$

Fig.9